LA-12427-T
Thesis

UC-910
Issued: November 1992

A Search for 100 TeV Gamma-Ray Emission from the X-Ray Binary Pulsar 4U 0115+63 Using the CYGNUS Extensive Air-Shower Array

Dimitris E. Alexandreas

Los Alamos National Laboratory
Los Alamos,New Mexico 87545

Contents

List of Tables

List of Figures

Acknowledgements

My course from the undergraduate degree in Athens to the doctoral degree here in Irvine has not been a straightforward one. Eleven years of graduate studies in this country amount to an appointment as a "tenured graduate student", as one of my collegues put it. This last week, trying to finish up the dissertation, I have constantly in mind the verses by Kavafis that remind to us that, when you set on your return journey to Ithaca, you should wish that it be long, full of experiences and knowledge. When you get to Ithaca, you will find the island poor, with nothing more to offer you. Ithaca offered you the nice journey ...

Either because it was the first time away from home for so long, or because it is a beautiful college town, Ann Arbor will always be in my heart. I enjoyed both the campus activities there and the academic teaching. Special thanks to Professor Norman Scott for him great job in teaching CPU logical design.

The Department of Physics at College Park has been a very hospitable place for me. Dr. Kyriakos Tsokos with his help in the beginning of my effort to study elementary particle theory, Professors Arnold Glick and Ellen Williams with their counseling when I was not doing well in this study and I was unhappy, Earlene Bradley, the "mother" of all the graduate students there, my colleagues Gaurang Yodh and Jordan Goodman, who were there with the CYGNUS project the moment I needed one, and my Italian teacher Camilla Russell you really made me fall in love with the language; all have played invaluable part to the fact that today I am happy with what I am doing and what I plan to do.

When I got to Los Alamos and started working on the CYGNUS project, I could not imagine how much I would get to like both the project and New Mexico. The beauty of both of them definitely contributed to my reluctance to finish quickly and leave. Many thanks to the support personnel and the fellow researchers in the laboratory, as well as to the MP Division of the Los Alamos National Laboratory for the hospitality they extended to me and the many other CYGNUS collaborators that are almost "permanently" in that beautiful corner of the Northwestern New Mexico.

I have enjoyed being a member of the CYGNUS group. The interaction with each and every member of the collaboration has been most educating to me. Instead of listing here the names of all the people, I would just refer you to the authors' list of our most recent publications. But I do want to single out certain people: Jeremy Loyd-Evans helped me in my first steps in a research group, both in the hardware as well as in the analysis of the data (his efforts to teach me pool, though, were less fruitful). My graduate-school-mate Brenda Dingus, with all her experience in building the experiment has been a valuable advisor to all of us. All of us, the garduate students in the experiment, we appreciate the patience of Scott Delay, especially when he had to fix things after we would mess with the hardware. Darragh Nagle and Bob Burman, thank you for all your help and advice. Gerry, thank you for all the help with the barycentering routines. I have

really gained a lot from the invaluable conversations with and directions from Todd Haines, Steve Biller, Cy Hoffman, Jordan Goodman and Guss Sinnis. I will really miss my colleagues and friends Vishwanath and Mike Stark; I hope we will see each other again sometime.

Yes, this is a count-down. My advisor Gaurang Yodh has played a decisive role in my career. He helped me start by giving me a project and making me happy this way, he continued with his support and advice all these years, understanding how happy I was being in New Mexico rather than coming to Irvine, and he really motivated me, pushed me, forced me into finishing the writeup of the dissertation, thus making it possible to go to Padova almost on time. Without his efforts I would still be doing analysis. Gaurang, I will not forget your help. You have been a true advisor. Thank you.

New Mexico and the CYGNUS collaboration have been a very important chapter in my life. I will do my best to keep it open. It will be easier to do so with CYGNUS. New Mexico has to compete with my love for southern Europe; let' s see which one will win. Lot' s of thanks to all of you.

ABSTRACT

A Search For 100 TeV Gamma-Ray Emission
From The X-Ray Binary Pulsar 4U 0115+63
Using The CYGNUS Extensive Air-Shower Array
by
Dimitris E. Alexandreas

A search has been performed for unpulsed and pulsed Ultra-High-Energy gamma-ray emission from the X-ray transient binary pulsar 4U 0115+63 over timescales ranging from one source-day to the entire data set. The motivation has been the detection at TeV energies of 4U 0115+63 by the Čerenkov telescope at Dugway, operated by the University Durham, The search has been perfomed in the database of the CYGNUS I extensive air-shower array that extends from April 1986 to March 1992, and contains 17,000 hours of data from the source direction.

In the search for unpulsed emission, the background is estimated by creating random events from the actually detected data-set, and the Li & Ma statistic is used to evaluate the statistical significance of a backgrounf fluctuation. The Rayleigh test and its power are employed in the search for pulsed emission.

No statistically significant evidence for emission can be found. No correlation with its 24-day orbital period can be seen. A 90% confidence-level upper limit on the unpulsed continuous flux from 4U 0115+63 above 130 TeV is $7.0 \times 10^{-15}\,\mathrm{cm}^{-2}\mathrm{s}^{-1}$. This value agrees with that of the Whipple collaboration but is at least one order of magnitude lower than other upper limits or claimed detections.

Chapter 1

Introduction

Very high energy astronomy can offer most useful clues in the study of cosmic-rays, in the development of astrophysical models, even in the study of very high energy particle interactions. The motivation for pursuing astronomy at these energies will be outlined in this chapter, along with the techniques used for observations. The system 4U 0115+63 to be studied will be presented on the basis of past observations.

The astrophysical models developed (Kiraly 1988; Harding 1990) cannot predict PeV emission from a system like 4U 0115+63 with large orbital separation. The motivation for this research stems from the claimed detections in the TeV range.

The second chapter presents the methods used in the search for a signal. The subsequent two chapters apply these methods to the search for unpulsed and pulsed emission from 4U 0115+63. The last chapter summarizes the results and compares them to past observations.

1.1 Motivation

It may not be just plagiarism but also frustration that many theses and reviews relevant to cosmic rays and gamma-ray astronomy start with a statement that, though

cosmic rays were discovered by V. F. Hess in 1912 (Hess 1912), their origin is still not clear. Do they come from point sources or not? In the highest energies where only ground based detectors are used, which detect only the secondary cascades in the atmosphere, what is the nature of the primary?

There has been unquestionable detection of very high energy radiation from the Crab nebula in the TeV energy region (Vacanti 1991). Detections have been reported from Cygnus X-3 in the TeV (Neshpor 1980) and PeV (Samorski & Stamm 1983a; Lloyd-Evans 1983) regions. There have also been other detections, at different levels of confidence, from Hercules X-1 in TeV (Dowthwaite 1984; Lamb 1988; Resvanis 1988) and PeV (Dingus 1988b) energies, Vela (Raubenheimer 1989), 4U 0115+63 (see section 1.3), and other "point" sources. Do all cosmic and gamma rays come from point objects? Using the luminosity detected from Cygnus X-3 in the 1-10 PeV energy region, which is comparable to that in X-rays (KeV), Hillas (1984) estimates for Cygnus X-3 the power in 10-100 PeV particles as $2 \times 10^{37} \mathrm{erg\,cm^{-2}\,s^{-1}}$, sufficient to supply the entire cosmic ray flux. But in the last few years no more positive detections of Cygnus X-3 have been made. What about extragalactic sources? The majority of observations so far have concentrated on galactic sources, but there have been some claims of detections of extragalactic ones (see review by Weeks 1988).

What is the nature of the primary entering the atmosphere? Since even singly charged particles with energies of 1 PeV have a gyroradius of 0.3 parsec in the 3 microGauss galactic magnetic field, and these point sources are several Kiloparsec away, there is no way that charged primaries could retain any sense of their point of origin. Therefore the primary has to be neutral in order to observe sources. Due to their life time, neutrons of even 1 PeV would decay within a few parsecs. Neutrinos do not have large enough interaction cross sections in the atmosphere to account for the observed fluxes. The most widely accepted candidate is the photon.

But there have been detections (Samorski & Stamm 1983b; Dingus 1988b) where the muon component of the secondary cascade indicated that, according to what we know about photonic interactions so far, the primaries from Cygnus X-3 and Hercules X-1 may not have been photons.

Astrophysics has a lot to gain from the study of cosmic rays: their composition depends on the site and mechanisms of their creation and acceleration, and the medium of propagation. The characteristics of cosmic radiation place constraints on theoretical models for the emitting system, be it interstellar medium or discrete sources. This dissertation studies 4U 0115+63, which is an example of X-ray binary sources. They consist of a neutron star a few Km in diameter and with a mass equal to 0.5 to 1.6 $M_\odot$ and a companion star with a mass about 1 to 50 $M_\odot$, orbiting at a distance up to a few hundred lights seconds. Due to the intense gravitational field of the neutron star, matter is flowing from the companion to the neutron star. If the companion has evolved to the stage where it fills its Roche lobe, matter flows to the neutron star through the first Lagrange point, gains significant angular momentum due to the rotation of the neutron star, and forms an ***accretion disk*** around it. Otherwise, matter flows from the companion in a stellar wind and may or may not form an accretion disk.

In the case of stellar wind, matter free falls into the neutron star up to the region where the energy density of the magnetic field of the latter becomes comparable to the kinetic energy of the falling matter. From then on the magnetic field forces the falling charged particles to corrotate with the neutron star and directs them to the polar regions. In the accretion disk case, turbulance and magnetic stresses are believed to govern the dynamics; particles eventually leave the disk for the star's poles.

The many models developed to explain or predict acceleration of particles to TeV and PeV energies can be grouped in two major categories. In the first one

revolution ?
magnetic axis ≠ rotation axis

(Kiraly 1988), shock mechanisms in the accretion columns near the poles create particle beams of up to 10^5 TeV. These get dumped on material in the accretion disk or on the companion, where they create pions that decay into photons, muons, electrons and neutrinos. Because of the neutron star rotation, the beam will sweep through the observer's field of view, resulting in a periodic signal. In the other model (see review in Harding 1990), acceleration is created by a potential difference induced by the rotation of the conducting accretion disk in the magnetic field of the neutron star. In this model, it is difficult to create a periodic signal. Regarding the acceleration site, the Haleakala, Whipple and Cygnus groups have detected VHE/UHE signals from Hercules X-1 all at the same period, which was different from the known X-ray pulsar period. This may imply that the signals originate from a region other than the surface of the neutron star.

The gamma rays and the charged cosmic rays created at those remote locations, arrive to earth with a spectrum extending up to PeV energies, providing a free beam for high energy physics. The problem is that the composition of the beam is not well known! As already mentioned, one of the main puzzles posed by this beam is the muon rich cascades apparently created by photons. Standard QED says that the muon to electron ratio is at least an order of magnitude less in a photon-initiated than in a hadron-initiated extensive air shower. This is in conflict with detections of Hercules X-1 by the Cygnus experiment, and of Cygnus X-3 by the Kiel and the Sudan Mine experiments. How do we explain the muon paradox? There is always the possibility of new physics involved in the production of muons in cascades initiated by photons. The existence of a new particle has been whispered, and people have talked about nuggets of quark matter, dibaryons (bags of six quarks), photinos, etc (Domokos 1988, 1989, 1990; Drees 1988, 1989).

1.2 Observations in VHE/UHE astronomy

The most common observation techniques in the radio through X-ray (KeV) part of the energy spectrum have been based on the detection of the primary signal coming from the source. At energies of 0.5 MeV to 10 GeV this has been done on satellites using telescopes constructed with scintillators, compton telescopes, spark chambers, e.t.c.

In the VHE (10 GeV - 100 TeV) and UHE (100 TeV - 100 PeV) part of the spectrum, though, the fluxes become so low (10^{-11}cm^{-2}s^{-1}) that it would take a year to get 3 events on a square meter of a satellite based detector! The easy solution is to use the atmosphere of the earth as a giant detector where the primary will interact and create a secondary cascade, an extensive air-shower (EAS), thus amplifying the area that the primary presents to the observing telescope. This way, though, we lose information about the nature of the primary.

There is no way we can detect the primary particle when the total thickness of air above sea level is 1033 g cm^{-2} and the photon interaction length is 37 g cm^{-2}. A primary 10 PeV gamma ray may result in about 10^6 secondary particles at detector level. Even so, we can still determine the properties of the primary: Because of its large energy almost all the momentum of the secondary particles is in the direction of the momentum of the primary. By using the orientation of the shower front and the total energy collected by the telescope, one can reconstruct the incident direction and estimate the energy of the primary.

Figure 1.1 shows schematically the components of an air-shower. A photon primary initiates an electromagnetic cascades. In the presence of atmospheric nuclei, it produces a pair of electrons which share its energy. Each electron radiates half its energy off via bremsstralung in the form of a photon which will in turn initiate another electromagnetic cascade. The number of quanta grows exponentially

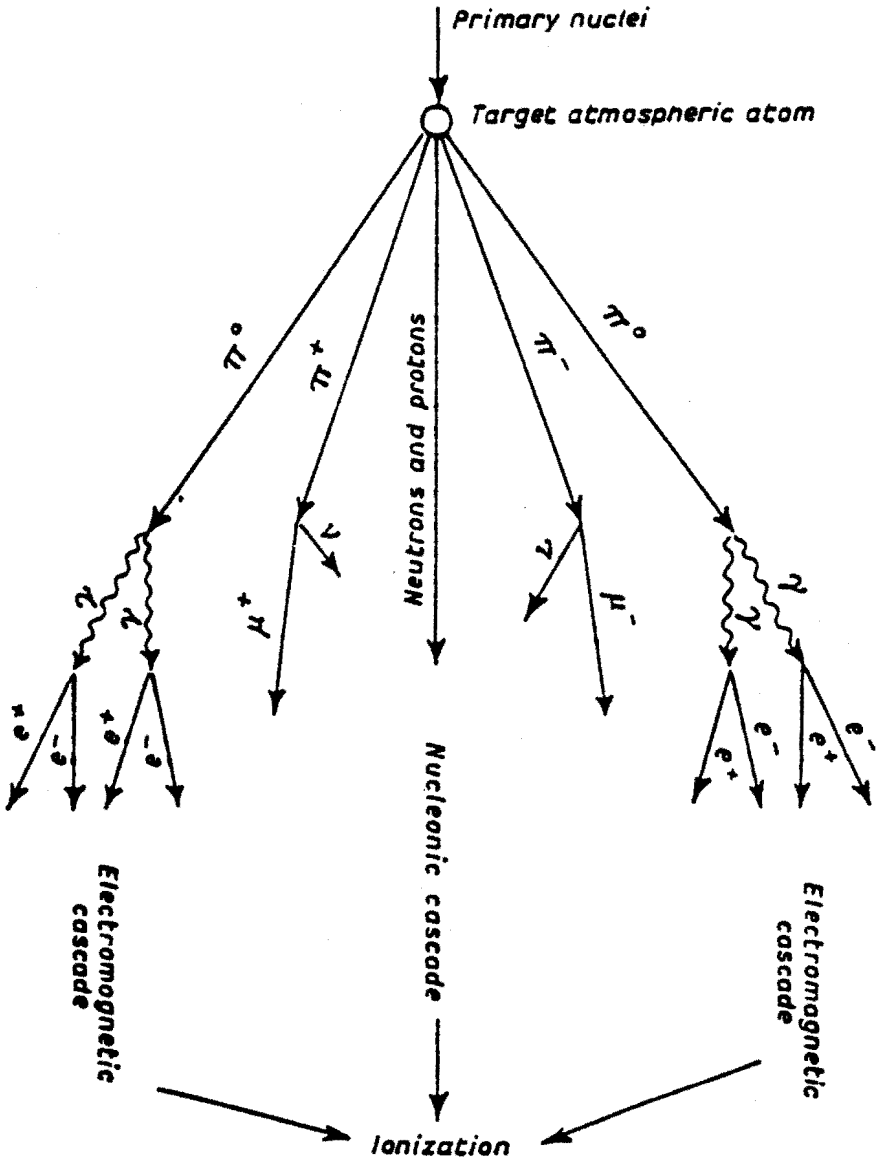

Figure 1.1: Basic elements in the development of the extensive air shower (Weeks 1988).

until the energy of individual electrons drops below 80 MeV; then ionization losses dominate and the number of particles starts decreasing off exponentially.

In a hadron initiated shower, the first interaction is with an air-nucleus, producing pions and secondary nucleons. The latter, and some of the charged pions, undergo further collisions with air-nuclei The rest of the charged pions decay to muons and neutrinos which survive to detector level. The neutral pions decay to gamma rays which initiate electromagnetic cascades. Thus the hadronic shower can be thought of as one with a nucleonic core which continually initiates small electromagnetic cascades. Its electron lateral distribution is not much different from that of a photon-induced shower. However, the hadronic shower develops further down in the atmoshpere and has fewer electrons and a larger muon component. Photons, too, can interact with nuclei, resulting in muons, but the cross-section of this interaction is three orders of magnitude smaller than that of e^+e^- pair production.

The charged secondary particles in the EAS produce Čerenkov radiation. Atmospheric Čerenkov telescopes detect this radiation using photomultiplier tubes at the focus of a set of mirrors. They can only operate during dark moonless nights with clear skies. Their acceptance is determined by the area covered by Čerenkov photons with high enough density. This fact limits the use of the technique to energies between 100 GeV and 10 TeV.

At energies above 10 TeV, where the secondary particles survive to ground level, observations are made via Extensive Air-Shower Arrays which sample the front of the shower by using a grid of detectors. Each detector consists of a scintillator that converts the shower charged particles into photons that get detected by one or two PMTs. If the time of arrival of the shower front at each detector can be measured to within a few nanoseconds, then the direction of the primary can be determined to within a few degrees. (Satellite based X-ray observations have angular resolution

of a small fraction of a degree). The CYGNUS experiment that acquired the data for this dissertation consists of such an EAS array.

1.3 The 4U 0115+63 Binary Pulsar

In September-October 1971 and in 1972-73 the Crimean Astrophysical Observatory made a series of 4.5 hour scans, in the drift-scan mode, centered on declinations +62° (Stepanian 1972). Among all the data sets collected, those of October 1971 and of December 1972 showed excesses of 3.9 and 3.6 σ, respectively, above the energy threshold of 2 TeV, from what they concluded to be a new variable discrete source. They called it *Cas Gamma-1* and its best position was right ascention $01^h\ 16 \pm 4^m$ and declination $+62° \pm 1°$. It was subsequently noted (Vladimirsky 1984) that, in the 100 MeV gamma-ray region, the SAS-2 experiment detected in March 1973 a source in this error box, whereas the COS-B experiment did not when observing at a later time.

4U 0115+63 was first identified as a variable X-ray source in the fourth catalog of the UHURU satellite. UHURU detected an outburst from a "new" source located at right ascention $01^h15^m13.8^s$ and declination +63° 28' 38" between December 1970 and March 1971 (Forman 1976). The source location is in the error box of the Cas Gamma-1. Since then, X-ray emission from 4U 0115+63 has been detected only sporadically in the form of bursts that occur every approximately three years and last for about one month (see review by Whitlock 1989). The sporadic nature of emissions and the positional coincidence strengthen the proposal that Cas Gamma-1 is the same as 4U 0115+63 (Stepanian 1972; Lamb 1986).

Pulsations at a period of 3.6 s have been detected in most of these observations. This, and other parameters of the binary orbit, like the orbital period P_{orb} of 24.3 days, the large eccentricity e of 0.34 and the long semimajor axis $a_x \sin i$

Parameter		Value
Projected semi-major axis	$a_x \sin i$	140.13 ± 0.16 lt-s
Orbital eccentricity	e	0.3402 ± 0.0004
Pulsar Period	P	3.614690 ± 0.000002 s
Pulsar Period Derivative	$\dot{P}/P$	$-(1.8 \pm 0.2) \times 10^{-4} yr^{-1}$
Periastron Passage Time	τ	JD 2,447,942.030 ± 0.006
Periastron Argument	ω	48.02° ± 0.11°
Orbital Period	P_{orb}	24.31535 ± 0.00005 days
Periastron Advance	$\dot{\omega}$	0.030° ± 0.016°

Table 1.1: Parameters for the 4U 0115+63 binary X-ray system (Rappaport 1978; Tamura 1992).

of 140 lt-s, were first identified and measured by Rappaport (1978) in the January 1978 burst of the source, recorded by the SAS 3 satellite. The average value of $\dot{P}/P$ during the burst implies an X-ray luminosity of 2×10^{36} erg s^{-1} and a distance of 2.5 Kpc. The values of P_{orb} and $a_x \sin i$ imply a mass of 5 $M_\odot$ for the companion, consistent with a main-sequence B star. Cyclotron emission lines indicate a magnetic field of 10^{12} G.

The most recent measurements of these parameters (Tamura 1992) come from the February 1990 burst detected by the satellite Ginga. In this determination, the values of $a_x \sin i$ and e were fixed to those by Rappaport (1978), and P_{orb} was determined by the time of the periastron passage τ in this and previous detections. The complete set of these parameters is shown in table 1.1. From 1970 to 1990 there appears to have been little net change in the pulsar period, suggesting that the outbursts of emission of X-rays coincide with episodic mass transfers from the companion to the neutron star and spin-up, interspersed by long quiescent periods

Group & Reference	Observation Duration	Energy Threshold	Burst Duration	Integral Flux $10^{-13}cm^{-2}s^{-1}$
[1]Crimea	'71 - '73	2 TeV	two months	3000, d
[2]Dugway	Sep '84	1 TeV	continuous	700, p
[3]Whipple	'85 - '88	0.7 TeV		<100, p
[4]Pachmarhi	Winter '86	1.5 TeV	2-3 hrs	270, p
[5]Gulmarg	'87 - '88	2 TeV	1950 s	1800, p
[6]Pachmarhi	Oct - Nov '87	1.5 TeV		<60, p
[7]La Palma	Sep - Oct '88	0.4 TeV	continuous	4400, p
[8]Plateau Rosa	Feb '82 - Dec '87	30 TeV		<41, d
[9]EAS Top	'88 - '89	150 TeV		<1.9, d

Table 1.2: Summary of past TeV observations of 4U 0115+63. ([1]Stepanian 1972; [2]Chadwick 1985; [3]Macomb 1991; [4]Bhat 1987; [5]Rannot 1990; [6]Acharya 1990; [7]Brazier 1990; [8]Morello 1990; [9]Aglietta 1990).

of compensating spin-down.

The first detection of the source in the TeV energy range was made with the atmospheric Čerenkov telescope at Dugway, Utah, by the University of Durham. Motivated by the similarities in the X-ray behaviors of Hercules X-1 and 4U 0115+63, and following their detection of Hercules X-1, they observed the source in the continuous tracking mode during September 1984 (Chadwick 1985). In order to fold the data in search of the 3.6 s period, the orbital parameters had to be extrapolated from the last X-ray detection four years ago. A search for a signal at the X-ray period of the neutron star periodicity search showed an optimum period of 3.61457 ± 0.00001 s with a 10^{-5} probability of being due to chance. The signal corresponded to a flux of 7×10^{-11}photons $cm^{-2}s^{-1}$ for energies > 1 TeV and appeared to be constant over the 9 days of the observation. The light-curve showed a single wide peak, like that for Hercules X-1.

Table 1.2 summarizes most of the past VHE-UHE observations of the source. All detectors are Čerenkov telescopes except the last two which are air shower

arrays. For positive detections, the duration of the emission is given. For the rest, the integral flux is an upper limit. In this last column, $d\,(p\,)$ indicates that the flux was calculated assuming a unpulsed (pulsed) emission. Detections have been made only by Čerenkov telescopes and only by searching for the neutron star spin period. No enhancement of the on-source counting rate over the background has ever been observed. The Tata and Haleakala groups did see emission from the source for short intervals of time. However even though their total observing times were longer and their energy thresholds lower than those of the Durham group, no steady pulsed emission was seen.

Chapter 2

The CYGNUS Experiment

The CYGNUS experiment (Alexandreas et al. 1992) consists of an array of 204 scintillation counters for the detection of extensive air-showers and of three shielded muon detectors. It is located around the accelerator beam stop of the Los Alamos Meson Physics Facility (LAMPF) in New Mexico (latitude 106.3° W, longitude 35.9° N) at an elevation of 2,134 m above sea level; this corresponds to an atmospheric overburden of about 800 g/cm^2. Figure 2.1 shows the layout of the entire CYGNUS array and the location of the muon detectors.

2.1 The Extensive Air-Shower array

The first part of the array, known as CYGNUS I, started operation in April, 1986, with 50 scintillation counters and one muon detector. Its deployment was completed in the summer of 1989 with 108 counters covering 22,000 m^2. The detector spacing varies from 7 m near the center of CYGNUS I to 20 m near its edges. This way the array is efficient over a wide range of energies. CYGNUS I collects data at 3 Hz.

The second part, CYGNUS II, was built in order to increase the collection area at higher energies; it started collecting data in the fall of 1990 with 96 counters

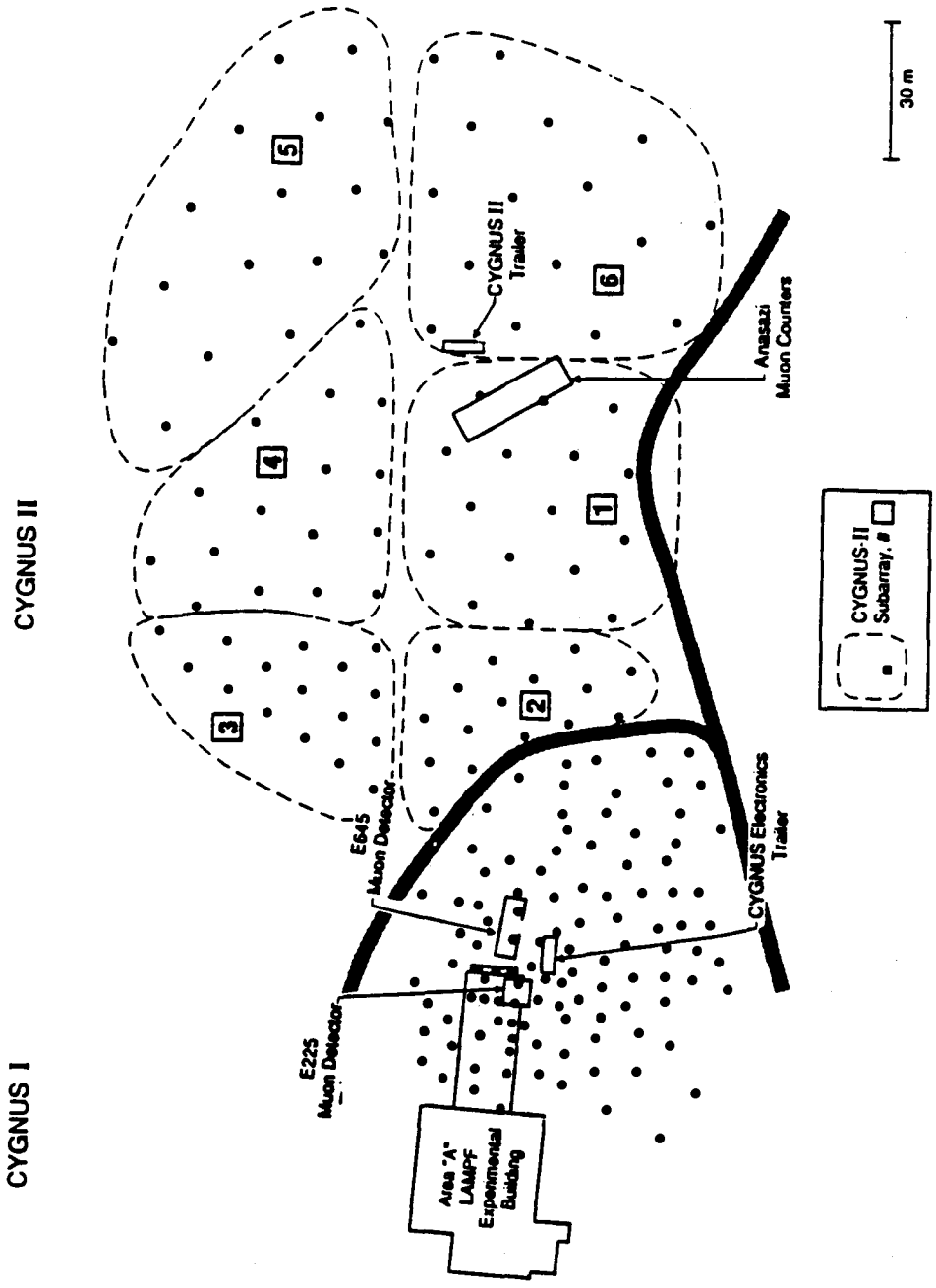

Figure 2.1: Locations of the CYGNUS scintillation counters and muon detectors.

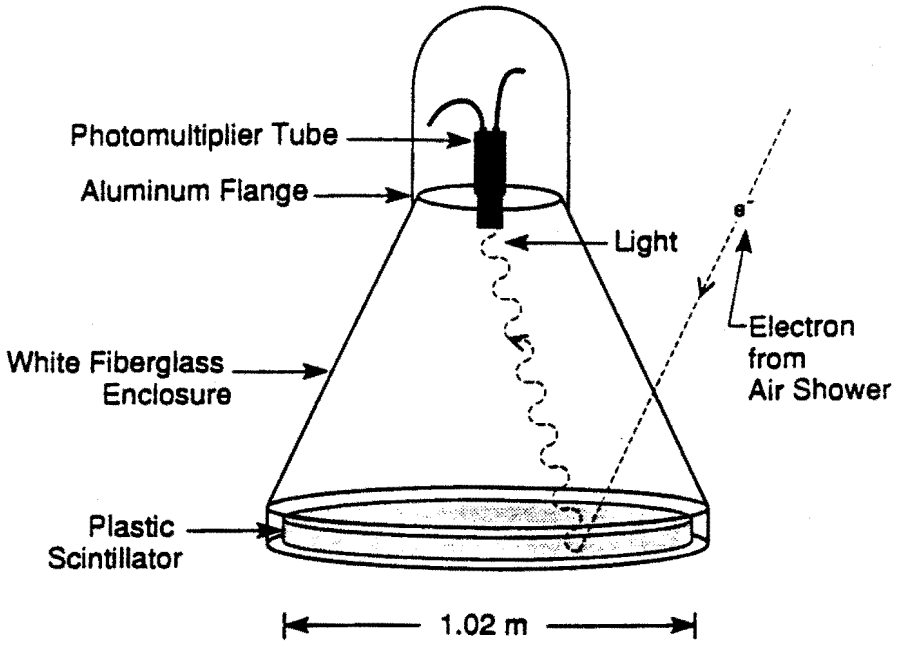

Figure 2.2: Schematic view of a CYGNUS scintillation counter.

over 62,000 m^2; their spacing varies from 20 m near CYGNUS I to 30 m. Its data rate is 1.8 Hz.

Each scintillation detector (figure 2.2) consists of a $\sim$ 1 m^2 piece of scintillator 0.1 m thick, viewed by a photomultiplier tube (PMT) in a light tight enclosure. The tube is $\sim$ 0.7 m away from the scintillator in order to minimize the spread of the photon transit times from the scintillator.

Since the summer of 1989, each detector has been covered with a 0.25 cm thick lead sheet which, at 60° to the horizontal, corresponds to one radiation length for normally incident particles. Its purpose is to convert the shower photons to electron pairs (see section 2.6).

The scintillator produces about 20 photoelectrons for each minimum ionizing particle. The photomultiplier tubes are the Amperex 2262, a 12 stage, high gain

tube, with risetime less than 2 ns. Their signals arrive at the electronics installation via RG-58 cables typically 70-150 m long. Pulse shape degradation and therefore time slewing due to the long cables is avoided by discriminating the signal at the level of 0.1 minimum ionizing particle after 10× amplification. These disciminated signals from the counters are then used as logic pulses in the multiplicity units that decide whether an air-shower has been detected (a trigger) and should be recorded. In the case of a trigger, the arrival time and pulse charge from each counter are digitized by 11 bit time-to-digital (TDC) and 10 bit analog-to-digital (ADC) converters on a CAMAC system.

All the electronics for CYGNUS I as well as the DEC μVAX II data acquisition computer for the experiment are located in a trailer in the middle of CYGNUS I.

The trigger specification for CYGNUS I is 20 counters firing within 300 ns of each other. This long coincidence window is dictated by the propagation time of the shower front across CYGNUS I for air-showers incident at large zenith angles.

A different scheme is adopted for CYGNUS II because of the long cable lengths necessary to cover its area. Its data acquisition electronics are located in a trailer in the middle of CYGNUS II, allowing cables typically 100-200 m long. The trigger systems of the two parts of the array exchange logic signals/instructions via an air-core 50 Ω cable, whereas the CYGNUS II CAMAC data get read out by the CYGNUS I CAMACs via a fiber optic link.

Because of the long cables, CYGNUS II is divided into 6 sub-arrays, each with 16 counters, its own TDCs and ADCs, and its own trigger of at least three counters firing. A triggered sub-array is read out in the case of a CYGNUS I or II trigger, the latter requiring any 16 CYGNUS II counters. Additional TDCs provide the relative timing among sub-arrays and between CYGNUS I and CYGNUS II.

Each counter is calibrated by recording its ADC and TDC values when the array gets triggered by particles (almost exclusively single muons) going through the

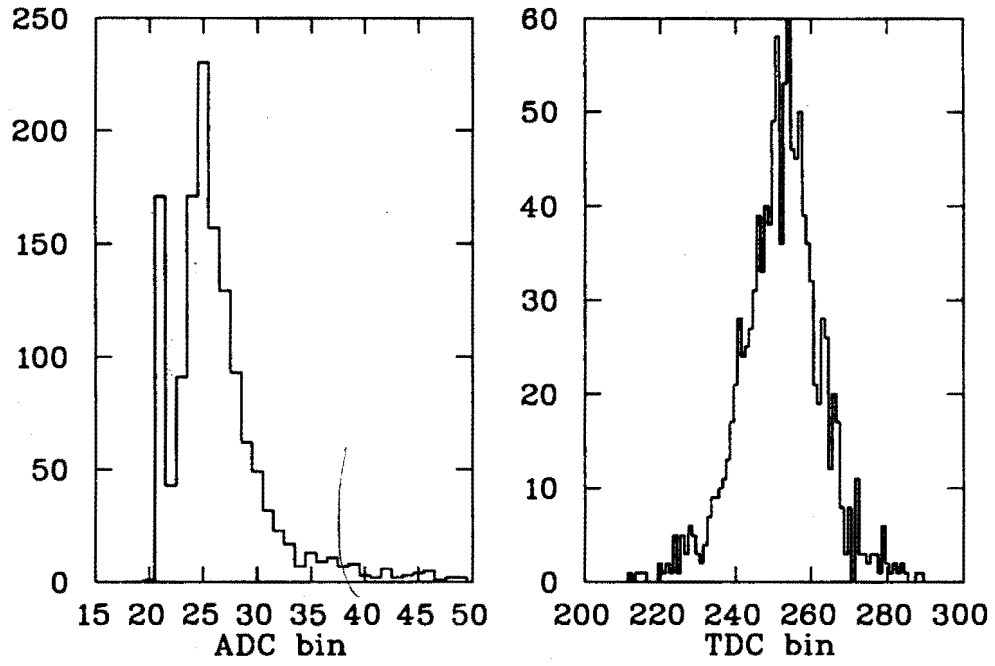

Figure 2.3: Sample scintillation counter calibration histograms.

detector. For this purpose, a small counter is used that consists of two overlapping 20 cm × 20 cm scintillator pieces, optically isolated from each other and each viewed by a photomultiplier tube. This calibration counter is placed in turn under each of the CYGNUS counters. Samples of the histograms collected for each counter are shown in figure 2.3. Instrument drifts dictate that calibrations be done a few times every year. During the interval between calibrations, the ADC pedestals get measured by triggering the array at random for a couple of minutes at the beginning of every run. Also the relative timing offsets of the counters get adjusted by the residuals of the fits of the arrival times to an air-shower front (see page 22 for explanation). By this procedure, the relative counter timing offsets are known to better than 1 ns rms and the array's absolute pointing direction is known to less than 0.2°.

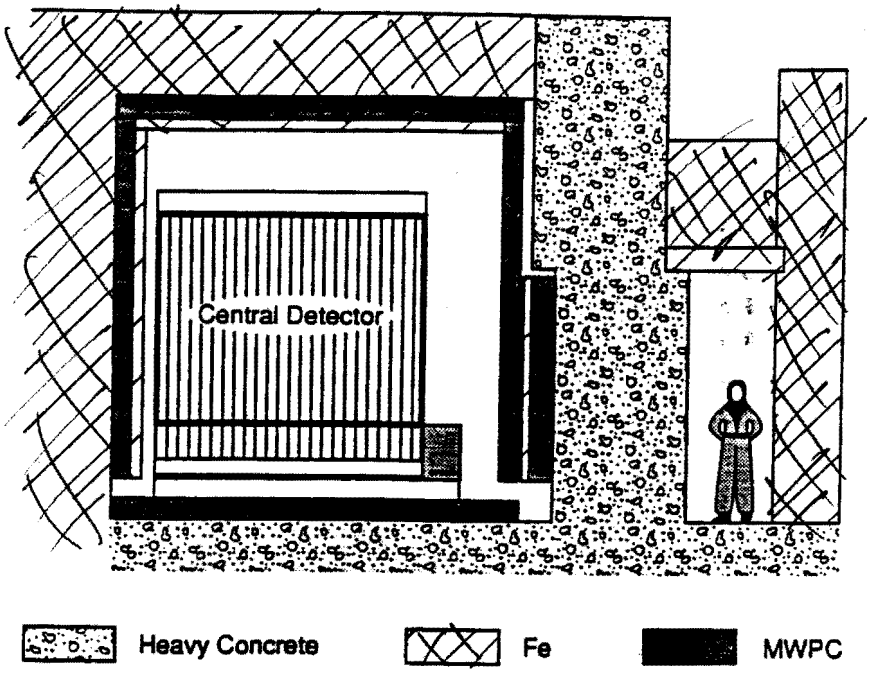

Figure 2.4: The E225 detector (used as muon detector for CYGNUS).

2.2 The muon detectors

CYGNUS uses muon detectrors in trying to discriminate between showers of hadronic and photonic origin.

The first such detector used was part of the past neutrino experiment E225 (figure 2.4) at LAMPF (Allen et al. 1992). The central detector of E225 consisted of scintillation counters and flash chambers forming a box $3 \times 3 \times 3.6$ m^3. It was used by CYGNUS even after the end of E255 running and until February 1988. It was then dismantled in order to use its scintillator for the CYGNUS II counters. E225 needed a veto against cosmic ray generated muons. Thus, the room it was located in was shielded by steel, concrete and earth at least 800 g/cm^2 thick, enforcing a 2 GeV minimun energy for muons penetrating it. The active veto used against

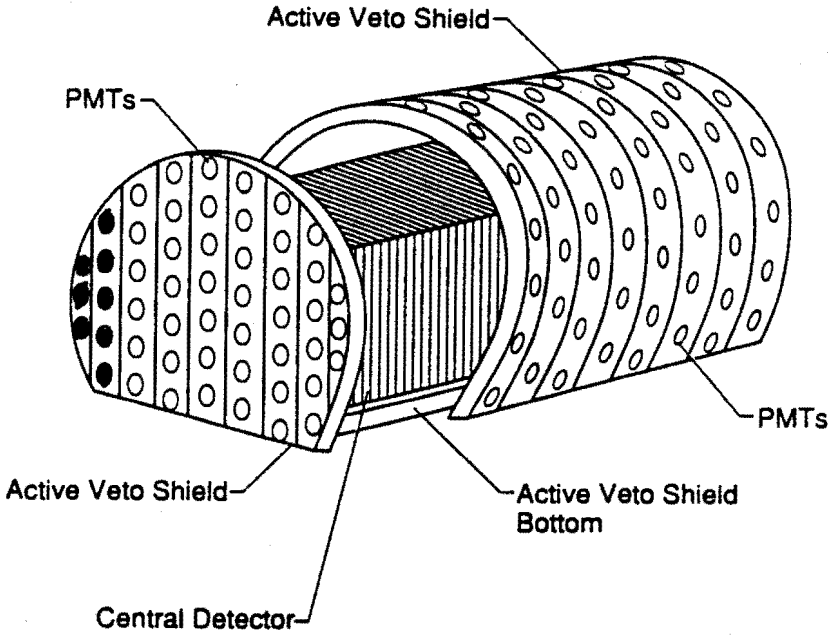

Figure 2.5: The E645 detector (used as muon detector for CYGNUS).

these penetrating muons consisted of layers of multiwire proportional chambers (MWPCs), each 5.4 m × 20 cm × 2.5 cm, covering the inside walls of the experiment area and forming a 6 × 6 × 6 m^3 cube; this presents an average area of 44 m^2 to incoming muons. The MWPCs have been used constantly. Their shape provides only coarse spatial resolution. A muon counting algorithm, though, works well for up to 7 muons and saturates at about 10. Their muon rate has dropped from 2.5 muons per CYGNUS event, when CYGNUS was small and surrounded E225, to 0.9 today.

Another muon detector is the active veto shield of the past neutrino experiment E645 (figure 2.5) at LAMPF. The shield consisted of 246 PMTs viewing liquid scintillator in the shielding tank. The earth and steel covering the detector location amount to an overburden of 2,000 g/cm^2. Its effective area for cosmic ray muons

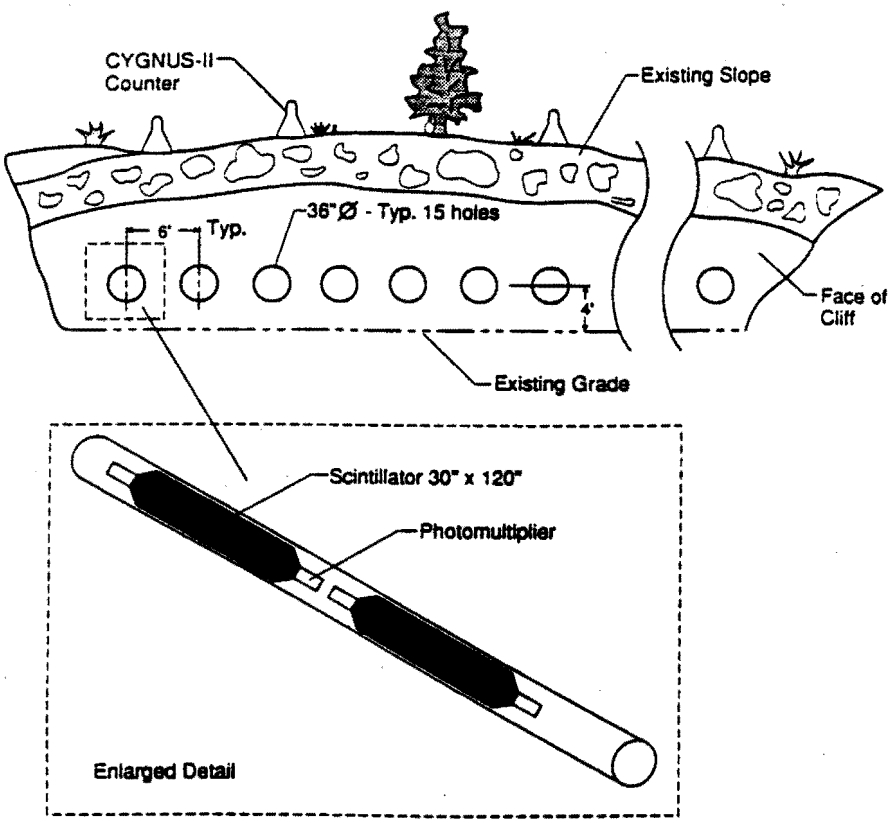

Figure 2.6: The Anasazi muon detector for CYGNUS II.

is 70 m^2. This detector, located under the north-eastern part of CYGNUS I, was used from January to May 1987 and from May to November 1990. It will be back in commission again in 1992 when the shield will be used by the upcoming neutrino experiment E1173.

The muon detector for CYGNUS II is located near its center and is named "Anasazi" after the cliff-dwelling Indians that lived in the area more than 600 years ago. It consists of scintillation counters (figure 2.6) burried under earth equivalent to 710 g/cm^2 of overburden. 30 scintillators, each viwed by two PMTs, provide an effective area of 70 m^2.

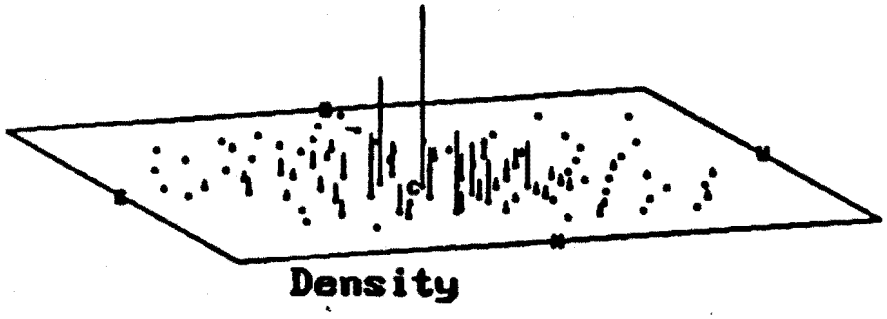

Figure 2.7: Pulse charges registered by counters for an air-shower event.

2.3 Event reconstruction

The data recorded for each event are used to calculate the characteristics of the primary particle that created the air-shower, most importantly its incident direction, arrival time, energy, and (wishful thinking) its nature.

In the determination of the incident direction of the air-shower front, one has to first know the shower core location, i.e. the place where the primary particle would have hit the ground if the atmosphere were not present. The core location algorithm uses a fit of the pulse charges registered by the counters (figure 2.7) to a two dimensional Gaussian. This is much less computer-time intensive than a four parameter fit to the Nishimura-Kamata-Greissen (NKG) formula (Greisen 1960) generally used to describe the lateral distribution of electrons in an air-shower.

Monte Carlo studies of the CYGNUS I configuration showed the error of this core location method to be less than 3 m near the center of the array and less than 8 m near the periphery. The error increases when the core is outside the array (according to Monte Carlo studies 16 % of the cores lie outside the array). In 8% of the events, where the detected particle distribution is dominated by one counter, the algorithm fails and then uses the hottest counter as the location of the core.

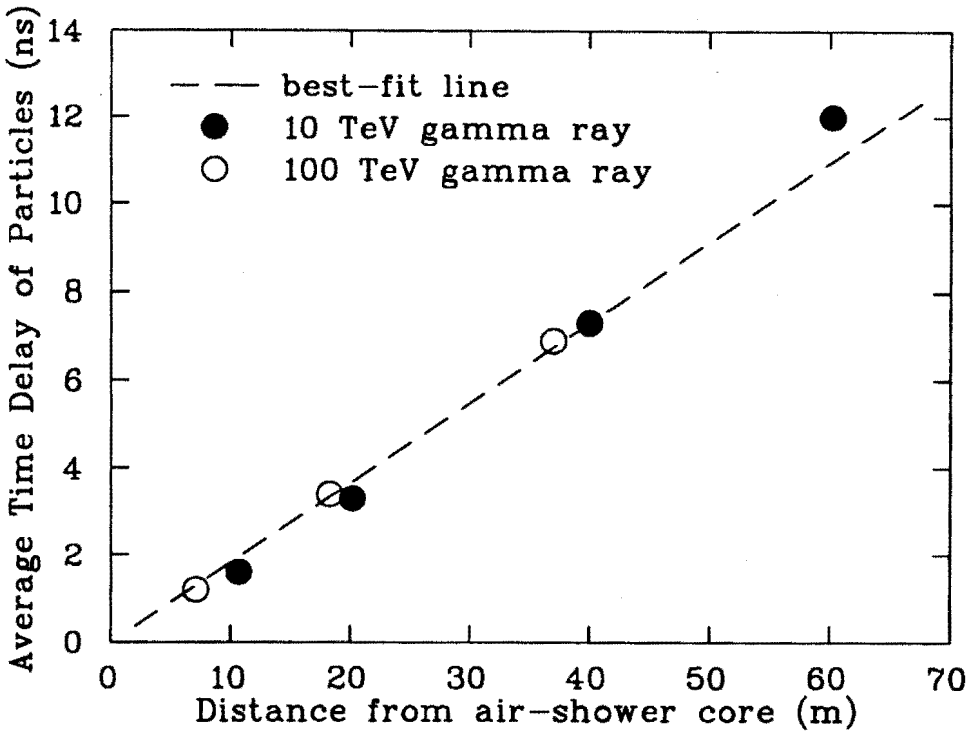

Figure 2.8: Monte Carlo calculation of the shower front curvature for gamma-initiated showers (no lead on the counters).

The incident direction is perpendicular to the shower front assumed to be planar. But due to the increased scattering of particles and to their lower density away from the core axis, the shower front has a thickness, and it is curved. Both the data and Monte Carlo simulations show that the average time delay of particles from the shower front (assumed to be a plane) due to this *curvature* can be parameterized by $C \times r \times N^{-1/2}$, where r is the distance of the counter from the shower core and N is the number of particles it registered. For the case of no lead sheets on the counters, and assuming gamma-initiated showers, figure 2.8 shows the result of a Monte Carlo calculation of this time delay as a function of the distance from the shower core, indicating a value of 0.2 ns/m for the curvature constant C (Dingus 1988b). This result is verified independently by using the data to estimate the

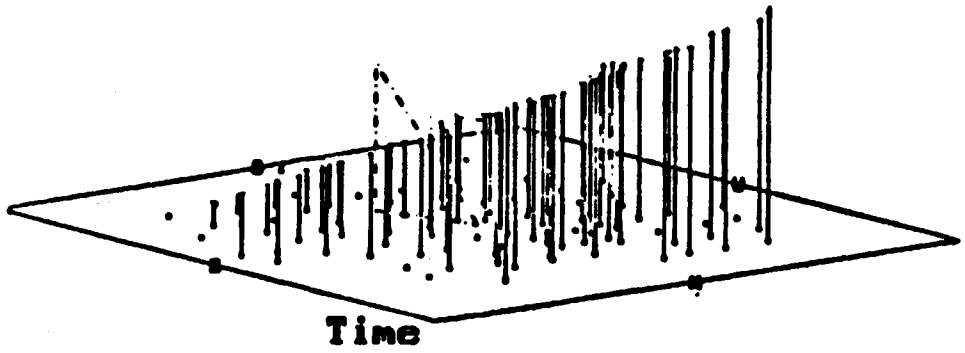

Figure 2.9: Curvature corrected relative arrival times to the counters for an air-shower event.

angular resolution of the array as a function of the value of C used when fitting the shower front to the incident direction. The angular resolution minimizes at the curvature of 0.2 ns/m. For the case of counters covered with lead, this value becomes 0.16 ns/m. The signal arrival times from the various counters are corrected by the amount of the curvature-induced time delay. These *curvature corrected* arrival times and the counter locations (figure 2.9) are used to fit the shower front to a plane using a χ^2 minimization method. The weight used for each counter in this fit is a function of the number of particles N: It is 0 for less than one minimum ionizing particle (MIP) registered, it becomes 1 for N greater than 5, and it is linear in N for $1 \leq N \leq 5$. This scheme has been determined empirically.

2.4 Angular resolution

In a search for point sources, the angular resolution of the instrument is essential in discriminating real signal from background, as will be explained in the following chapters. One way to estimate the resolution and the pointing accuracy of a gamma-ray telescope at these high energies is through the shadowing of cosmic rays by the

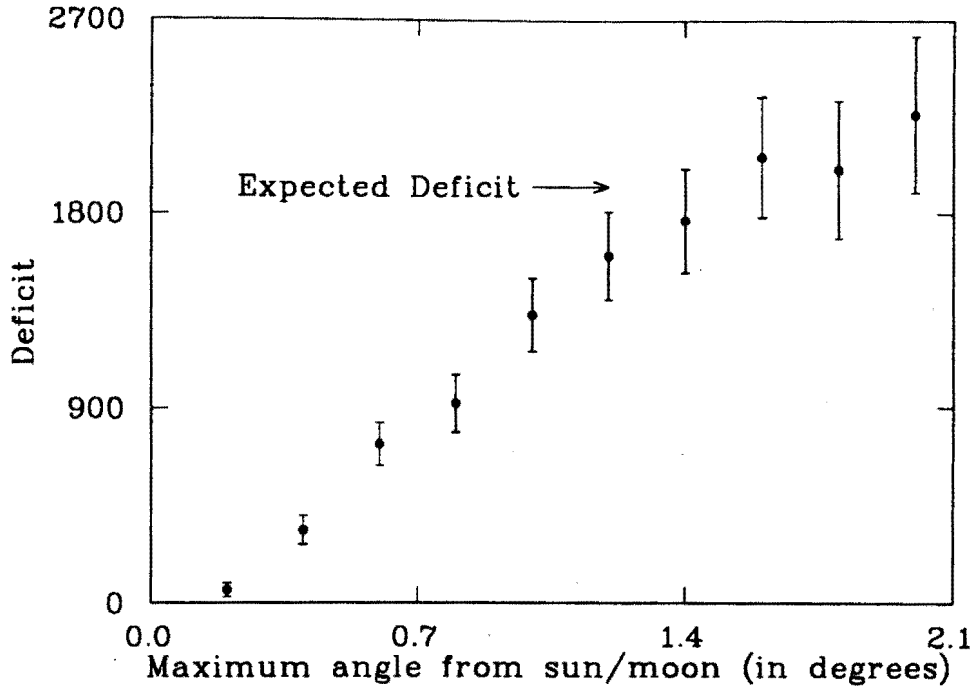

Figure 2.10: The deficit of events near the sun/moon due to the shadowing of the cosmic rays.

sun or the moon (Alexandreas et al. 1991a). Given that both these objects have an angular radius of about 0.26°, and that the angular resolution of CYGNUS, as estimated by other crude methods, is about 0.8°, a lot of data is needed to observe such a shadow at a statistically significant level. The shadow can be observed if one compares the number of events observed in a circle of given radius around the sun/moon to the number of events expected in that circle, as estimated from areas far from the sun/moon. Their difference, the deficit, is plotted in figure 2.10 as a function of the radius of the circle centered on the sun/moon. The expected deficit is indicated in the figure. This is an integral plot and, therefore, the errors are correlated.

The angular resolution is estimated by a maximum likelihood method. Each event near the sun/moon is assigned a probability of observing it; this probability

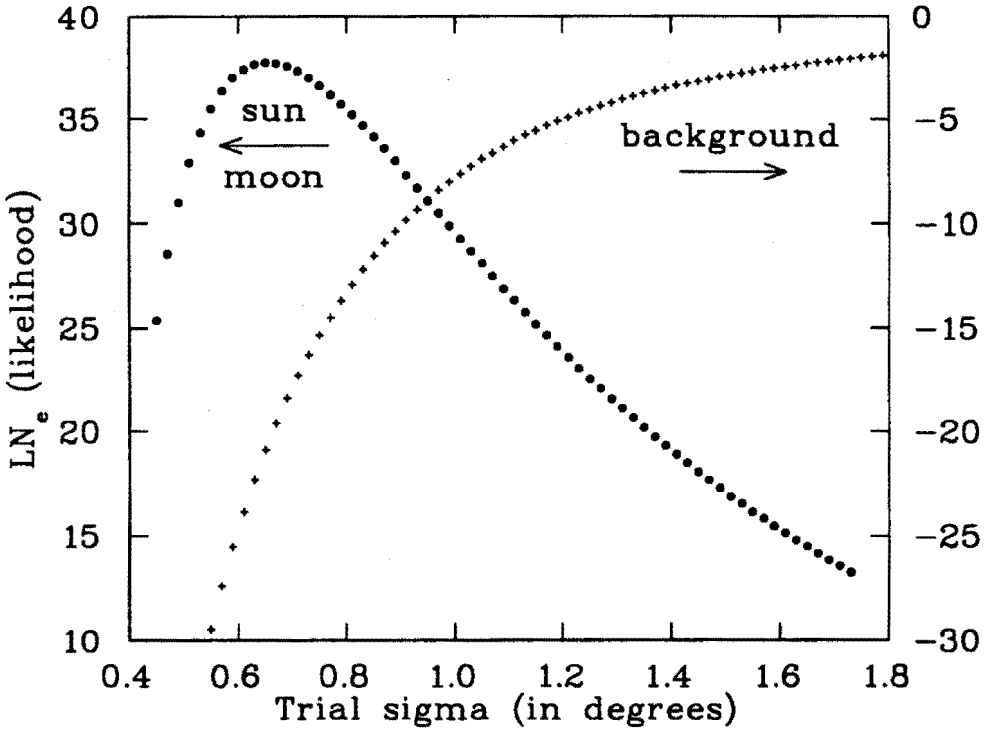

Figure 2.11: The likelihood of events vs. the assumed angular resolution of the experiment for data near the sun/moon (filled circles) and for data far from the sun/moon (crosses).

is a function of the event's angular distance from the sun/moon, and of the angular resolution of the experiment. The form of the resolution is assumed to be a two dimensional Gaussian, with its standard deviation σ as the measure of the angular resolution. The likelihood, defined as the product of the probabilities of all the events up to a radius of 5°, should have a maximum at the correct angular resolution. Figure 2.11 shows that the likelihood for data near the shadowing objects peaks at 0.67°, whereas for data away from the sun/moon it peaks, as expected, at large values of σ.

The angular resolution has been studied as a function of various cuts on the data. Table 2.1 shows the most dramatic dependences, i.e. on the total number of particles in the event and on the core location.

Data Cuts	No. of Events	σ (degrees)
No Cuts	145,435	0.67 + 0.07 - 0.07
Nptot > 200	23,197	0.37 + 0.08 - 0.05
0 < Nptot < 60	70,325	0.84 + 0.91 - 0.12
Core Inside Array	100,018	0.64 + 0.08 - 0.07
Core Outside Array	45,500	0.73 + 0.17 - 0.16

Table 2.1: Dependence of the angular resolution on the total number of particles Nptot in the event and on the core location.

2.5 Energy threshold and effective detection area

The energy threshold and the effective detection area of an air-shower array are quantities essential for the calculation of fluxes (see section 3.4). The energy threshold depends on the counter sizes and density, the trigger requirement, and the slant depth for each event (the atmospheric overburden the air-shower has to go through). This last quantity is a function of the elevation of the experiment above sea level, the incident zenith angle of the air-shower and the local air pressure. For a very nonuniform array like CYGNUS, the energy threshold also depends on the core location. Figure 2.12 shows the energy distribution of the events recorded by CYGNUS, as calculated by simulations assuming that all showers are initiated by protons. Monte Carlo studies show that for proton-initiated showers the energy threshold is 30% higher than it is for gamma-ray showers.

The effective area of the array depends on the same quantities as the energy threshold and also on the energy of the primary. It can be estimated by a Monte Carlo simulation of the development of air-showers in the atmosphere and of the response of the array to these showers. A total number of N_{tot} simulated showers are thrown over an area A_{tot} much larger than the area over which showers can

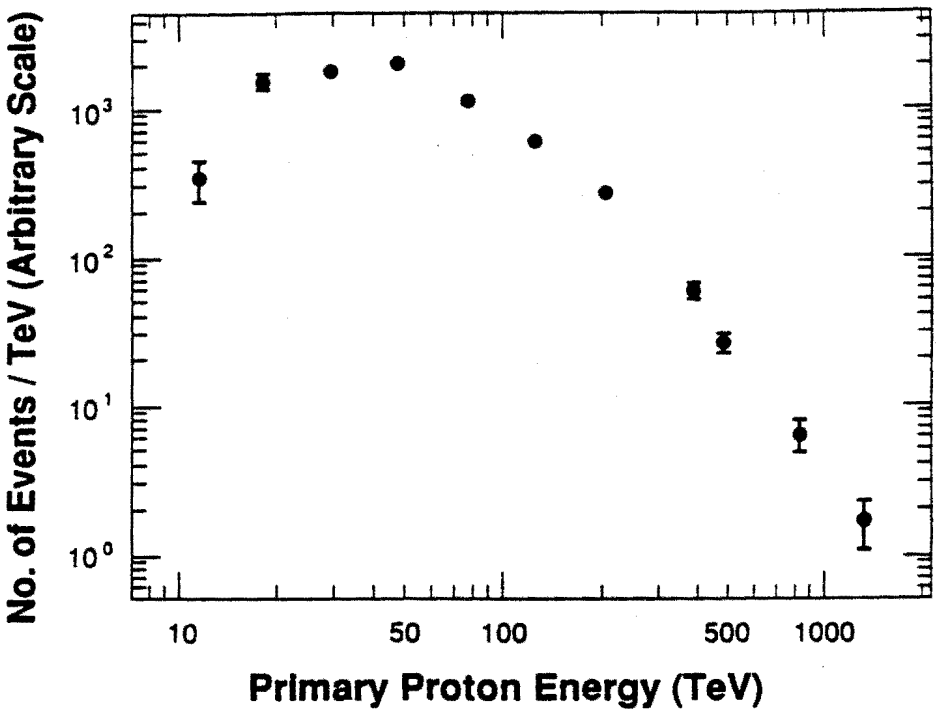

Figure 2.12: The energy distribution assuming the CYGNUS events are initiated by protons.

trigger the array. If $N_{\rm trig}$ is the number of these showers that do trigger the array in this simulation, then the effective area is $A_{\rm eff}(E,\theta) = A_{\rm tot}N_{\rm trig}/N_{\rm tot}$. The success of the method depends critically on the various air-shower and array properties being simulated correctly. Figure 2.13 shows the effective area of CYGNUS I, calculated this way and assuming a proton primary.

2.6 The effect of lead on the scintillation counters

The scintillator in the counters detects only charged particles. If the counters are covered with lead sheets, the air-shower photons get converted there into electron pairs and get detected by the scintillator. This increases the number of particles

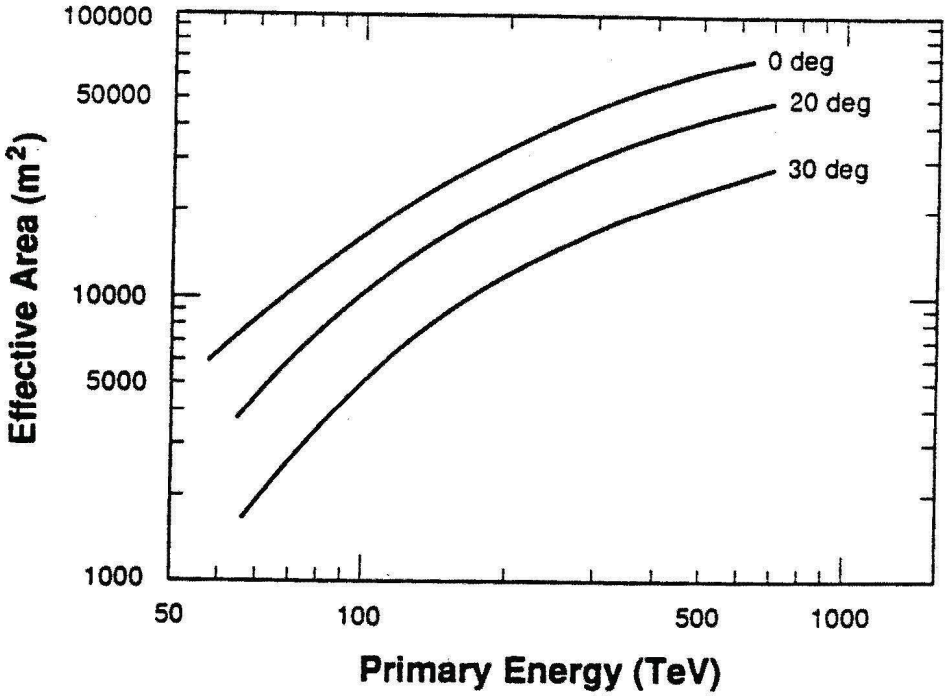

Figure 2.13: The effective area of CYGNUS I for proton primaries, calculated by Monte Carlo.

detected in each counter and, therefore, improves the timing and the angular resolution of the array (Linsley 1987; Bloomer et al. 1988; Amenomori et al. 1990). The detection of the shower photons also lowers the energy threshold of the experiment by allowing the reconstruction of showers with smaller size.

Since the summer of 1989, each detector has been covered with a 0.25 cm thick lead sheet which, at 60° to the horizontal, corresponds to one radiation length for vertically incident photons. The result is that 25% more particles get detected in showers, therefore allowing reconstruction of showers with 25% smaller size. The fact that by detecting photons, too, counters register more particles results in a lower curvature correction (0.16 ns/m) needed before fitting the air-shower to an incident direction. The data also show that the addition of lead on the counters

improved the angular resolution by 26%.

Chapter 3

Methods of Search for Emission

In most cases of reception, the signal of interest is mixed with and has to be separated from unwanted signal that constitutes the noise (background). In VHE/UHE gamma ray astronomy the signal from either an extended region in the sky like the galactic plane, or from a point source like 4U 0115+63, arrives at the telescope along with the isotropic flux of cosmic rays which is the background. In this part of the energy spectrum the signal to noise ratio is generally much less than one and, therefore, careful estimation of the background is crucial before characteristics of the real signal can be determined. Moreover, since the process involves a statistical estimation, the results are quoted giving the confidence level for the signal to be a random fluctuation of the background. This chapter presents the general procedure followed to extract the signal characteristics from the data and to calculate this confidence level.

3.1 Testing the Hypothesis of Emission

The mixture of the signal, if any, from an astrophysical object, and of the background, is estimated by looking for a period of time at a region in the sky where

the (suspected) source is located. This results in a number N_{on} of *on-source* events, the air showers with primaries originating from the direction of the source. The background alone is estimated by looking for comparable periods of time at regions of the sky away from the source. This results in N_{off} *off-source* events. A *test* of a hypothesis of emission from the source employs a *test statistic* which is a function of the on-source and off-source data sets. That yields the *significance level*, the probability to falsely reject the *null hypothesis* H_0 and accept the *alternate hypothesis* H_A. Under H_0 there is no source in the on-source sky region, and the on-source set of events is just another estimate of the isotropic cosmic ray background. In other words, the significance level is the probability that the on-source data set is a fluctuation of the cosmic ray background. By taking into account the efficiency of the telescope for receiving a signal from the on-source sky region relative to the efficiency for the off-source region, and the durations of observation and the sizes of these two regions, N_{off} can be used to estimate N_B (see next chapter for the method), the number of background events expected, under H_0, in the on-source data set.

The following alternate hypotheses of emission from 4U 0115+63 are tested in this dissertation:

H_1 There is ***unpulsed emission*** from the source: enhancement / excess of the on-source counts N_{on} over the background N_B.

H_2 There is ***pulsed emission*** from the source: phase alignment of the arrival times of the on-source events at the pulsar period of 4U 0115+63.

In each of these two emission searches ($i = 1, 2$), three sub-hypotheses are tested:

H_{i1} Daily emission: there is an episodic emission over the timescale of one ***source-day***. A source-day is one-sidereal-day long and it is centered at the time of

the source transit over the telescope. Assuming uninterrupted operation of the telescope, the source-day is the longest interval of continuous observation of the source.

H_{i2} There is an episodic emission over Timescales Varying from a few days to long subsets of the available data.

H_{i3} There is continuous emission over the entire data set.

These hypotheses form H_A. The Li & Ma statistic (see section 4.2) will be used to test for unpulsed emission and the Rayleigh statistic (see section 5.2) for pulsed emission.

In the search for daily emission there are about 2000 source days in the whole data set. The data of one day is independent of the data of the others. The test for emission is applied to each day. Let us assume that p_{min} is the *pre-trial* lowest (best) probability that the test yields for one of these $N_{tr} = 2000$ trials. Then the *post-trial* probability that among 2000 days at least one so improbable (under H_0) day will be observed is $P_{final} = 1 - (1 - p_{min})^{N_{tr}}$. If more trials are taken, P_{final} is larger, and the confidence level at which H_0 can be rejected is lower.

In the search for emission over variable timescales (Biller 1992) one divides the entire data set in non-overlapping consecutive windows of a chosen length (multiple of one source day, e.g. two days) and applies the test to each one of them. Since it is possible that emission will not be centered in one such time window, the sequence of windows is shifted by a fraction of the length of one window, and the test is applied again. This shifting is repeated until the sequence starts repeating itself. The best probability is chosen among the results for all these windows, and gets multiplied by the appropriate trials factor (see below) to get the p_{min} for this timescale. Then the data is divided in longer time windows and the procedure applied again in order to get the new p_{min} and choose the best between this one and

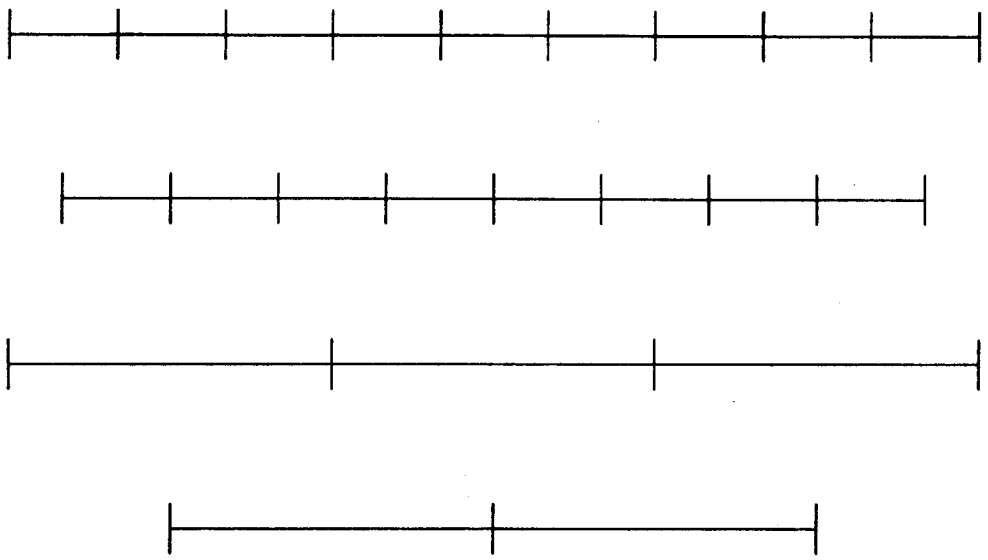

Figure 3.1: Time windows used to search for emission over arbitrary timescales.

that for the previous timescale, and so on. The P_{final} has to take into account also the fact that more than one timescales have been tried. This procedure is shown pictorially in figure 3.1. The more relative window offsets and different timescales are tried, the higher the trials penalty factor N_{tr} will be. This factor has to be determined by Monte Carlo simulations tailored to the particular test since not all of these windows contain independent data. This work has been done by Biller (1992). It has been found that the following is a good compromise between increasing the trials and increasing the sensitivity of the method, i.e. the chance to find a window that results in a very low P_{final}: Windows of a given duration should be offset only once by half their length. The trials factor for the best probability p_{min} for this set of windows is the number of independent windows (e.g. about 1000 for 2-day windows in our data set) times the factor given in the following table (depending on the statistic used) for the fact that one offsets the windows. Then the length of the windows should be increased by 3. The last trials factor for trying various

Li & Ma statistic	$1.8 - 0.775 p_{\min}{}^{0.356}$
Rayleigh statistic	$1.96 - 0.46 p_{\min}{}^{0.256}$

timescales is 1 for the first timescale plus 0.5 for each additional one.

3.2 Bin Size and Shape

In a search for a weak directional signal the bin size should be chosen such that it maximizes the signal significance determined through the test statistic, e.g. the value of the Li & Ma S or of the Rayleigh power. Due to the finite resolution of the telescope, assumed for CYGNUS to be a two dimensional Gaussian with its standard deviation σ as the measure of the angular resolution, the signal from a point source will be spread angularly following a Gaussian distribution; the background events are expected to be uniformly distributed at least over a small area of the sky. Then, in the case of large values of $N_{\rm on}$ and $N_{\rm B}$, and for at least the test statistics used here, the optimum bin is the one that maximizes the Poisson significance of the excess of $N_{\rm on}$ above $N_{\rm B}$. The optimum angular radius r for a circular bin centered on the direction of the point source is the solution to the following equation (Dingus 1988b):

$$\frac{d}{dr}\left(\frac{1-\mathrm{e}^{-r^2/2\sigma^2}}{r}\right) = 0$$

The signal significance maximizes at $r = 1.59\sigma$. Such a bin will on average contain 72% of the source signal; therefore part of the source signal will end up in bins neighboring the source one.

In the case of low statistics, Monte Carlo studies (Biller 1992) show that the optimum radius r is given by the following table, where N is the number of background events expected in a circular bin of radius 1σ. Figure 3.2 shows graphically

Li & Ma statistic	$\left(1.59 + 0.713e^{-0.876N^{0.36}}\right)\sigma$
Rayleigh statistic	$\left(1.59 + 7.4e^{-2.286N^{0.145}}\right)\sigma$

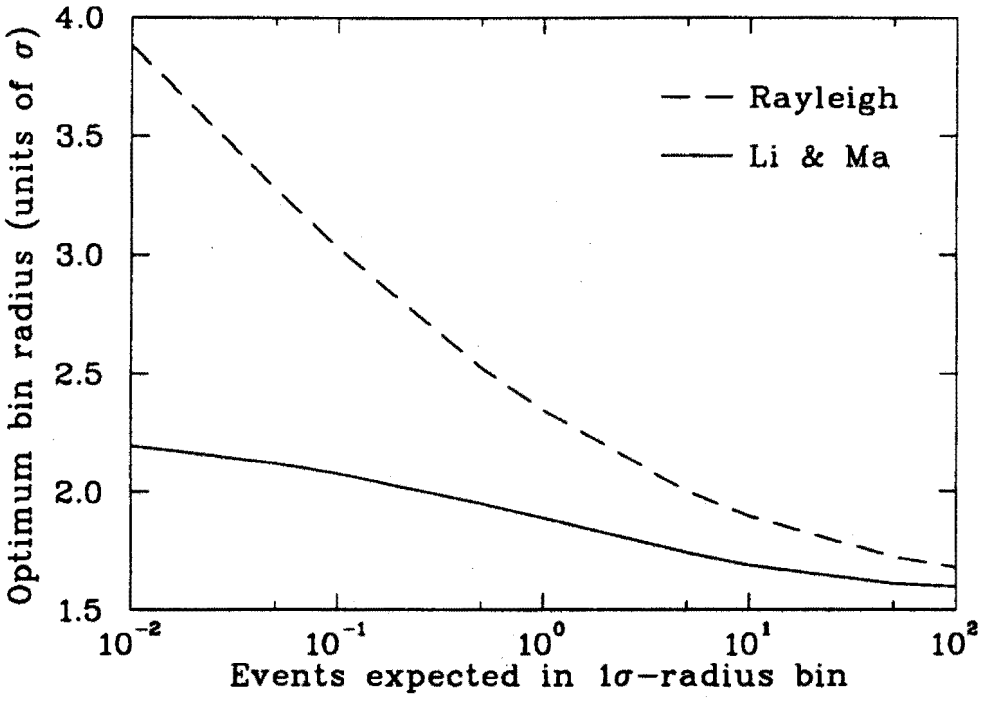

Figure 3.2: The radius of the bin that optimizes the signal significance for the Li & Ma statistic and the Rayleigh statistic in units of the angular resolution σ as a function of the number of events expected in a circular bin of radius 1σ.

these relations.

Square bins that have the same area as the optimum circular bin are, according to simulations, almost as good as the circular bin in optimizing the signal significance, and they are much easier to implement computationally. The on-source region used here will be a bin which is square in the local coordinates, is centered on the source location, and its side has an angular width $\Delta\delta = \sqrt{\pi}\, r$, r being the optimum bin radius. The dimensions of this bin in the celestial sphere coordinates will be $\Delta\delta$ in declination and $\Delta\alpha = \Delta\delta / \cos\delta_s$ in right ascension, where δ_s is the

declination of the source.

3.3 Applying the Tests for Emission to the Data

The data set used in this dissertation spans the interval from April 1986 to March 1992. There are 2200 source days in this interval, but, due to gaps in the data acquisition, 140 of these do not contain any data for 4U 0115+63. Only the events that have triggerred CYGNUS I (and may be some subarrays of CYGNUS II) will be used in the analysis presented here. The angular resolution of purely CYGNUS II events in still under investigation. A large square bin 4.5° in declination is used in order to select the on-source and the expected off-source events that will be used for further processing. The set of expected off-source events is estimated each source day by the randomization procedure explained in page 43. Figure 3.3 shows the number of expected off-soure events in each source day for which data is available. The step-increases are due to the changes in the experiment (lead deployment, more counters, e.t.c.) that increased the data rate. Spikes towards lower values are due to partially lost exposure because of down time (run changes, equipment malfunction, calibrations). The off-source events of consecutive days can be combined in order to estimate the background for time intervals which are multiples of one source-day.

The data set prepared as explained in the previous paragraph is then divided in time windows of appropriate length according to the hypothesis being tested. In the search for daily emission, consecutive non-overlapping one source-day long windows are used. In testing for emission over arbitrary timescales, two source-days long windows are tried first, then six day ones, and so on, until a long time window is reached that includes all the data (continuous emission). For a given time window the bin optimum for the appropriate test (Li & Ma or Rayleigh) is calculated based on the number of off-source events in the window, and then the test is applied to

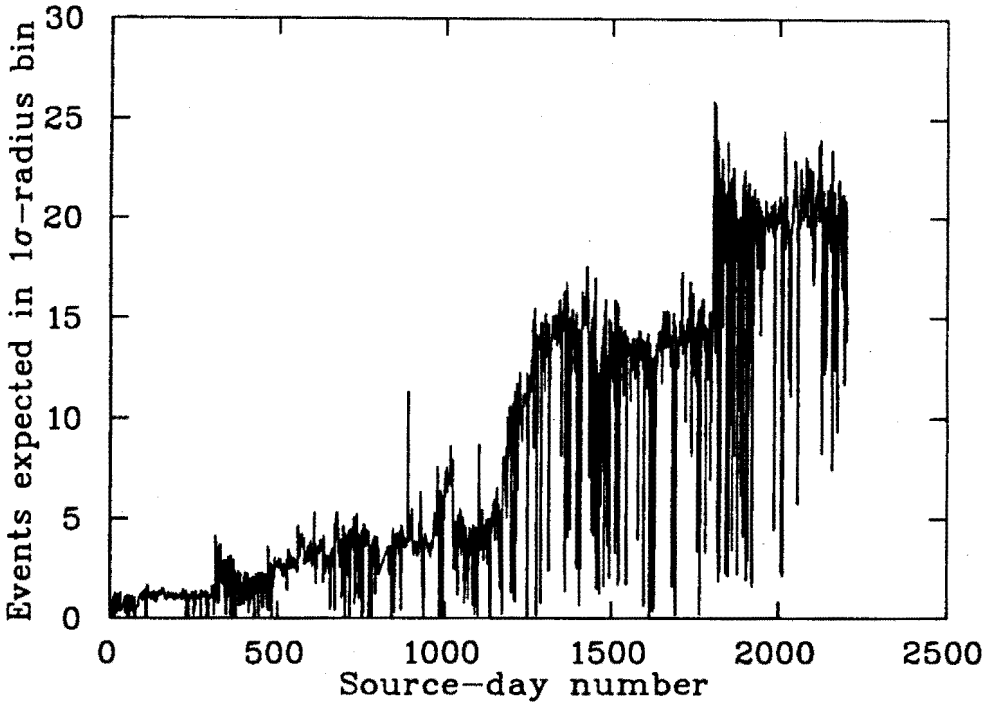

Figure 3.3: The number of background events expected in each source day, in a circular bin of radius 1σ centered on 4U 0115+63, calculated by the randomization procedure explained in page 43.

the on-source and off-source events in the optimum bin. The results for all the time windows under a given hypothesis are compared to what is expected under H_0. The next two chapters present these results of the searches for unpulsed and pulsed emission.

3.4 Calculation of Fluxes and Flux Upper-limits

The major species which make up the cosmic-ray primaries are usually grouped as follows: protons, helium, C-O, Ne-S, and Fe. The last group includes all primaries with atomic weight of at least 25. The number N_{cr} of background cosmic-ray showers observed from a particular off-source region of solid angle $\Delta\Omega$ in the sky

can be written as:

$$N_{cr} = \Delta\Omega \sum_i \int \frac{dF^i_{cr}}{dE} A^i_{cr}(E, \theta(t)) dE dt,$$

where θ is the zenith angle of the sky region $\Delta\Omega$ at the observation time instant t, the index i runs over the four cosmic-ray species, and for each of them: dF^i_{cr}/dE is the differential flux of that species, and $A^i_{cr}(E, \theta(t))$ is the effective area for air-showers created by that species. The flux can be written as:

$$\frac{dF^i_{cr}}{dE} = C_i E^{-\gamma_i}$$

where C_i is a constant and γ_i is the spectral index.

The total number N_{gr} of gamma-ray events from a point source in the sky can be written in a similar way:

$$N_{gr} = \int \frac{dF_{gr}}{dE} A_{gr}(E, \theta(t)) dE dt,$$

where $dF_{gr}/dE = C_{gr} E^{-\gamma_{gr}}$ is the differential gamma-ray flux.

C_{gr} can be calculated by:

$$C_{gr} = \frac{N_{gr}}{N_{cr}} \Delta\Omega \sum_i \frac{C_i}{R_i}.$$

R_i is the trigger efficiency of the air-shower array to gamma rays from a point source relative to that for isotropic cosmic rays of the species i:

$$R_i = \frac{\int E^{-\gamma_{gr}} A_{gr}(E, \theta(t)) dE dt}{\int E^{-\gamma_i} A^i_{cr}(E, \theta(t)) dE dt}.$$

Then the integral gamma-ray flux above energy E expected from the source is: $F_{gr}(> E) = C_{gr} E^{1-\gamma_{gr}}/(\gamma_{gr} - 1)$.

In the absence of any other indication in the data, a soft gamma-ray spectrum has been assumed with $\gamma_{gr} = 2.76$, the same as that for protons. The value of R_i has been calculated by Monte Carlo for protons. Figure 3.4(a) shows its dependence

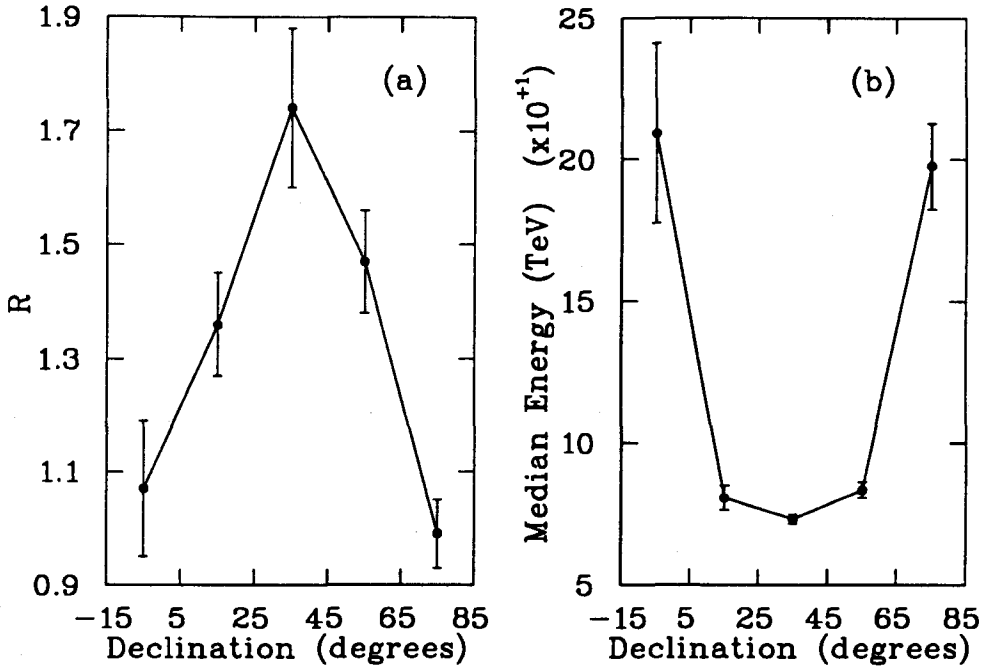

Figure 3.4: The sensitivity R to gamma-rays relative to protons, and the median energy of the expected gamma-ray spectrum vs. the declination (for CYGNUS I, by Monte Carlo).

on the declination of the point source for the CYGNUS I array. R is 1.25 for 4U 0115+63. The expected integral gamma-ray fluxes or their upper-limits will be quoted above the median energy of the gamma-ray spectrum expected to be observed by CYGNUS I. Figure 3.4(b) gives this median energy vs. the declination of the source for CYGNUS I, calculated by Monte Carlo. It is 130 TeV for 4U 0115+63. For protons $C_i = 9.17 \pm 2.39 \times 10^{-6}\,\mathrm{cm^{-2}s^{-1}sr^{-1}TeV^{-1}}$, and $\gamma_i = 2.76$ (Burnett 1990). Therefore: $F_{proton}(> 130\mathrm{TeV}) = 9.9 \times 10^{-10}\,\mathrm{cm^{-2}s^{-1}sr^{-1}}$.

A square bin with a side of angular width $\Delta\delta$ casts a solid angle $\Delta\Omega = (\Delta\delta\ \pi/180)^2$. In this bin we observe $N_{cr} = N_{\mathrm{B}}$. Because of the finite angular resolution σ, the bin contains only a fraction ϵ of all the events N_{gr} emitted from

the source. Therefore $N_{gr} = (N_{\rm on} - N_{\rm B})/\epsilon$, where:

$$\epsilon = \left[\int_{-\Delta\delta/(2\sigma)}^{+\Delta\delta/(2\sigma)} \frac{e^{-x^2/2}}{\sqrt{2\pi}} dx\right]^2 .$$

When the confidence level is too low to reject H_0, the formula will be used to calculate a 90% confidence-level upper-limit of the signal flux from 4U 0115+63. This means that, since one cannot be 100% sure that the true value of N_{gr} is 0, an upper limit $N_{90\%}$ will be calculated such that, if the experiment is repeated many times, then in 90% of the cases the calculated $N_{90\%}$ will be higher than the true (unknown) N_{gr}. The reader is reminded, though, that various quite different approaches to such a calculation are used in the scientific community, and comparisons of results from different experiments are possible only if the same method of calculation has been used. The reader is, therefore, encouraged to use the results $N_{\rm on}$ and $N_{\rm B}$ of the analysis presented in the subsequent chapters, and apply the method of his taste for deriving fluxes.

The procedure adopted here for calculating $N_{90\%}$ is that of Helene (1983). In the cases presented here, the gaussian approximations can be used for both the signal and the background distributions because $N_{\rm on} \gg 1$ and $N_{\rm B} \gg 1$. Then $N_{90\%}$ is the solution to the equation

$$\alpha = I\left[\frac{N_{90\%} - (N_{\rm on} - N_{\rm B})}{\sqrt{N_{\rm on} + N_{\rm B}/n}}\right] / I\left[\frac{-(N_{\rm on} - N_{\rm B})}{\sqrt{N_{\rm on} + N_{\rm B}/n}}\right],$$

where

$$I(z) = \int_z^\infty \frac{e^{-x^2/2}}{\sqrt{2\pi}} dx,$$

is the error function, n is the ratio of the size of the off-source region used in estimating $N_{\rm B}$ to the size of the on-source region, and $1 - \alpha = 0.9$ is the confidence level.

Chapter 4

Search for Unpulsed Emission

This chapter presents the background estimation method and the results of the search for unpulsed emission, that is for enhancement / excess of the on-source counts N_{on} over the background N_B (see previous chapter). The Li & Ma S statistic used is also presented here. In this counting method the efficiency of the telescope for receiving a signal from the on-source sky region relative to the efficiency for the off-source region must be well known. The most important reason for this consideration is the fact that the efficiency of an EAS array depends dramatically on the zenith angle. Figure 4.1 shows the number of events received during a CYGNUS data run as a function of the zenith angle. The assumption of azimuthally symmetric efficiency made in figure 4.1 is not true in a very non uniform array like CYGNUS where the scintillator counters are arranged in a non-uniform grid (see figure 2.1), and not located on a single plane. The efficiency has also short-term variations due to the atmospheric conditions since the atmospheric burden over the telescope depends on the pressure, and long-term variations due to the various upgrades of the telescope.

The easiest way to overcome the problem of proper efficiency estimation, is to ensure that the strength of the background is estimated from off-source regions

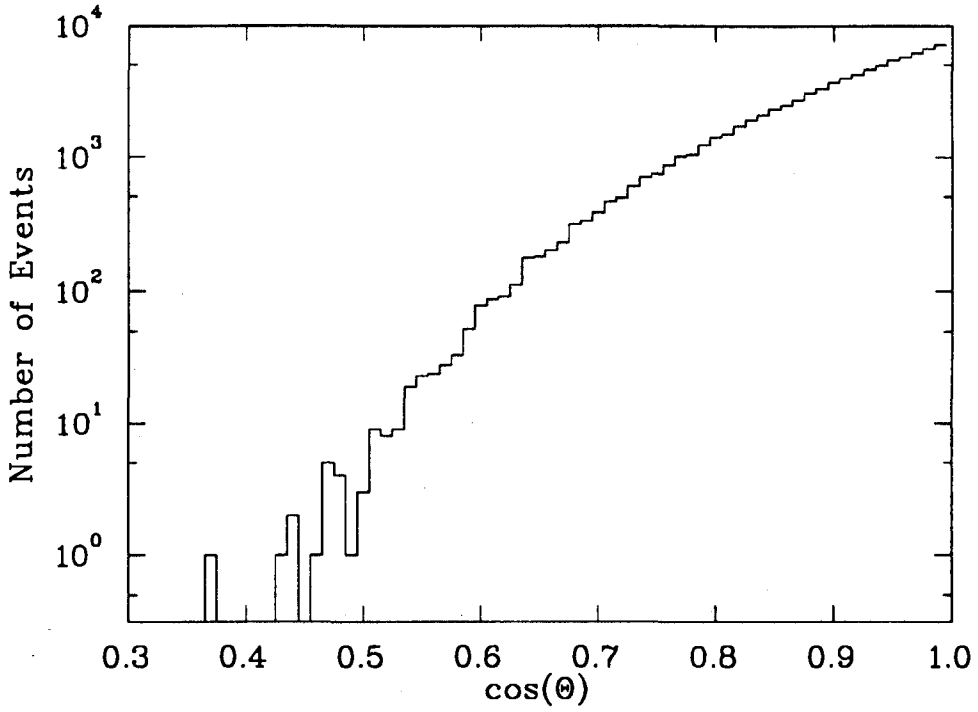

Figure 4.1: Histogram of CYGNUS data events vs. the cosine of the zenith angle.

that have spent the same length of time as the on-source region at any given zenith angle in the local sky. From here on the phrase *local sky* will be used to express the system of the local zenith and azimuthal (θ, ϕ) coordinates at the site of the telescope.

4.1 Background Estimation

The CYGNUS collaboration has gone through three main variations of a *right ascension scanning* method in trying to deal with this problem. The starting idea is to choose bins (regions) in the celestial sphere that have a given declination (DEC) and that are spread over various right ascensions (RA). The trajectory of these bins in the local sky is a circle due to the rotation of the earth. Therefore, these bins are

all going to spend the same time at any of the zenith elevations they go through. Typically for a point source, the *source-bin* is centered on the RA and DEC of the source, and a number of non-overlapping *background bins* of the same shape and size (see section 3.2) are chosen adjacent to (e.g. five to the east and five to the west of) the source-bin. The numbers of air-showers arriving from these bins are used as the best estimate of the on-source and off-source number of events. Having the same number of background bins on either side of the source takes proper care of any telescope efficiency changes that are linear in time. The drawback of this simple implementation manifests itself when the experiment is not collecting data due to a run change or hardware failure (efficiency changes that are non-linear in time). The effect of these *down times* is that if data collection resumes (stops) when any of the bins are above the horizon, then some of them will start (stop) at lower zenith angles than others. This results in them having different effective exposures to the various parts of the local sky.

The attempt to correct this problem enforces that events will be counted in the bins only when they originate from the parts of the local sky that all the bins have gone through. This implementation is facilitated by the use of the *hour angle* (HA) of a point in the celestial sphere. At any given time, the HA is the difference between the RA of the zenith over the telescope and the RA of the point of interest. The HA effectively expresses the time it will take for the point we are interested in to arrive at the meridian of our location on earth. Therefore, in our RA scan method where we enforce an *equal exposure HA cut*, we calculate the maximum HA among our sky bins at the time the experiment resumes operation and their minimum HA when data aqcuisition stops. We enter into the bins only those events that have HAs in this range. The major disadvantage of this method is that it rejects a lot of data. The length in RA of the rejected HA range is that of the arc comprised by the on-source and background bins. The more background bins we use on each side of

the source and the higher the declination of the source (see section 3.2 for bin size), the stricter this HA cut becomes. As an example, using four background bins on each side of the source-bin, the method rejects 20% of the data for a source at the declination of HERCULES X-1 (it transits almost at the zenith over the telescope) and 50% for 4U 0115+63 (it transits about 30° from the zenith). An improvement of this HA cut method avoids this problem of data rejection by using either fewer background bins altogether, or fewer bins on one side and more on the other side of the source-bin when the experiment stops or resumes operation (Dion 1992). The first solution increases the uncertainty whereas the second cannot accomodate even linear changes in the telescope efficiency.

The two implementations of the RA scan method that have been described above also suffer of other problems which are independent of the down times of the telescope. Short-term event rate variations due to local air-pressure changes (weather conditions) or due to hardware malfunctioning, and long-term rate changes due to detector upgrades, result in variations in the effective exposure to different parts of the local sky. Selection of background bins on both sides of the source-bin can correctly estimate the background only if these efficiency changes are at most linear in time.

The third improvement of the RA scan method appears to be dealing correctly with these problems if carefully used. It is the one that is being used for the data analysis presented in this dissertation. It will be described next, along with the various tests done to check its performance and reliability in estimating the background.

TIME SLOSHING

The method uses all the events acquired in the time interval during which we search for unpulsed emission, and creates at random new, fake, events which constitute the background and which preserve the (t, θ, ϕ) distribution of the real events. This is accomplished as follows. For every real event, a new arrival time

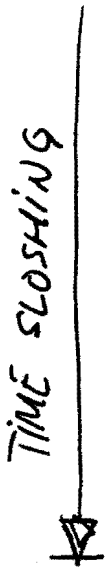

is selected among the set of times of all the events. The new event is to have arrived at the new time but from the same local sky point (θ, ϕ) as the real event. Since the selection of a new time amounts to a rotation of the celestial sphere with respect to the earth, this method changes only the right ascension of the event but not its declination. Rotation of the original RA by the amount equivalent to the difference between the new and the real time of the event results in the RA of the new, background, event. For better estimation of the background, ten new events are created for each real event. The off-source data set for a given source is then the set of fake events which end up in the source-bin, and $N_B = N_{off}/10$.

4.2 Estimation of the Significance of a Result

Once a given method is used to get the best estimate of the number of events on-source, N_{on}, and off-source, N_{off}, the presence (or absence) of a signal is usually estimated through the statistical significance of the excess (or deficit) $N_S = N_{on} - N_B$ under the H_0 hypothesis. According to this hypothesis, there is no source in the on-source sky region, both N_{on} and N_B are estimates of the isotropic cosmic ray background and, therefore, the expected value of N_S is 0. The confidence level is the probability (also expressed in Gaussian standard deviations) that $N_{on} - N_B$ fluctuated to its observed non-zero value. The estimation has to take into account the Poisson statistical fluctuations that govern the observed N_{on} and N_{off}. This can be done numerically by using a double integral over N_{on} and N_{off} (see discussion in Haines 1986); it gives statistically correct answers, but it is computationally very time-consuming. The procedure adopted here was introduced by Li & Ma, 1983, and accomplishes analytically by maximum likelihood the same goal as the double-integral numerical calculation of the Poisson significance; it is, therefore, much faster and also easier to implement. It expresses the significance in terms of

the variable S given by

$$S = \sqrt{2\left\{N_{\rm on}\ln\left[\frac{1+\alpha}{\alpha}\frac{N_{\rm on}}{N_{\rm on}+N_{\rm off}}\right] + N_{\rm off}\ln\left[(1+\alpha)\frac{N_{\rm off}}{N_{\rm on}+N_{\rm off}}\right]\right\}},$$

where α is the ratio of the on-source to the off-source observation times. For example, in the search for unpulsed emission we determine $N_{\rm off}$ from 10 off-source bins, each having the same size as the on-source bin; then $\alpha = 1/10$.

In the case of the null hypothesis, and if $N_{\rm on}$ and $N_{\rm off}$ are not too few (more than 10), the distribution of S will approximately follow that of the absolute value of a standard normal variable; the larger the $N_{\rm on}$ and $N_{\rm off}$, the better the approximation. S can be considered negative if $N_{\rm on}$ is less than $\alpha N_{\rm off}$, positive otherwise. The Gaussian distribution can be used to calculate the probability that an observation $(N_{\rm on}, N_{\rm off})$ is produced by background. The quality of the Gaussian approximation has been tested by the following simulation. $\alpha = 1/10$ is assumed. Then an expected number $\langle N_{\rm off}\rangle$ is chosen, and, under H_0, $\langle N_{\rm on}\rangle = \alpha\langle N_{\rm off}\rangle$. Two random numbers $N_{\rm on}$ and $N_{\rm off}$ are generated from Poisson distributions with expectations $\langle N_{\rm on}\rangle$ and $\langle N_{\rm off}\rangle$ respectively. The significance S of the simulated observation $(N_{\rm on}, N_{\rm off})$ is calculated and histogrammed. This simulation is repeated 10^7 times for the chosen set of α and $\langle N_{\rm off}\rangle$. A Gaussian probability distribution function is fitted to the resulting histogram of S, and the mean μ, the standard deviation σ, the number of events in the distribution, and their errors are determined from the best fit. Table 4.1 shows the dependence of these fitted parameters on $\langle N_{\rm on}\rangle$. Even though for small values of $\langle N_{\rm on}\rangle$ the distribution of Li & Ma S cannot be approximated by a Gaussian, S is still a very good estimate of the significance of positive excesses. This can be seen in figure 4.2 where the histogram is the distribution of S for the case $\langle N_{\rm on}\rangle = 1$, and the curve is the Gaussian distribution with mean 0 and variance 1 that is expected from the number of entries in the histogram.

$\langle N_{on} \rangle$	μ	σ
5	0.034	0.8785
10	-0.044	1.0068
10^2	-0.014	0.9996
10^3	-0.0047	1.0004
10^4	-0.0017	1.0005
10^5	-0.00067	1.0005
10^6	-0.00043	1.0005

Table 4.1: Gaussian best-fit to the Li & Ma S distribution. The statistical error is ± 0.0003 for μ and ± 0.0002 for σ.

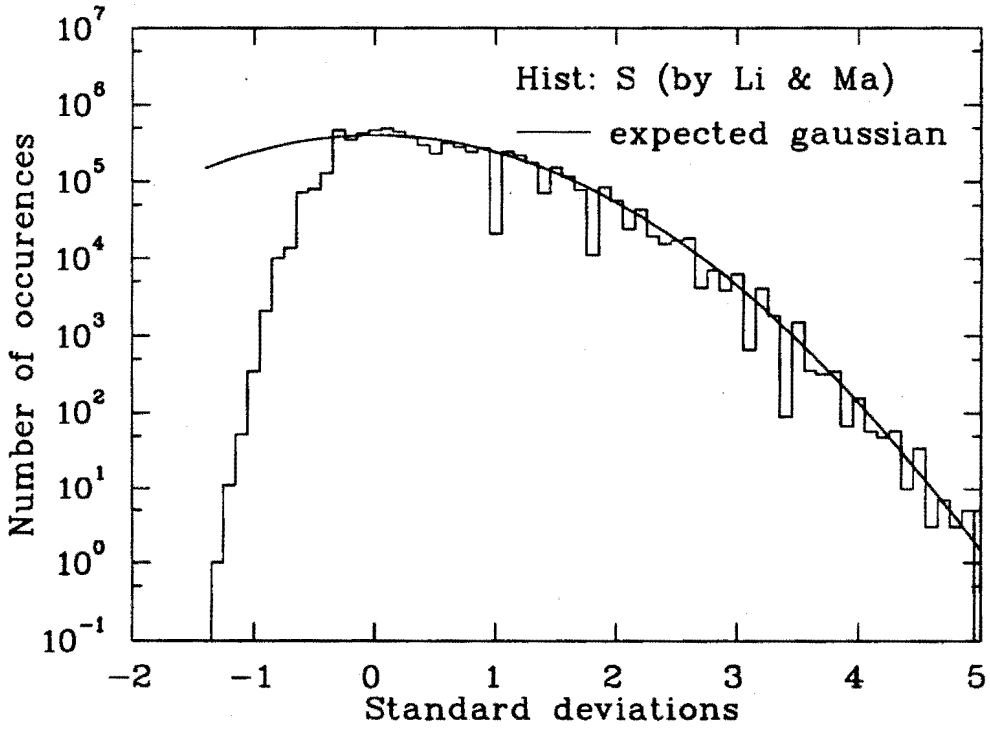

Figure 4.2: Distribution of the Li & Ma S for $\langle N_{on} \rangle = 1$. The superimposed curve is the standard normal distribution normalised to the number of trials.

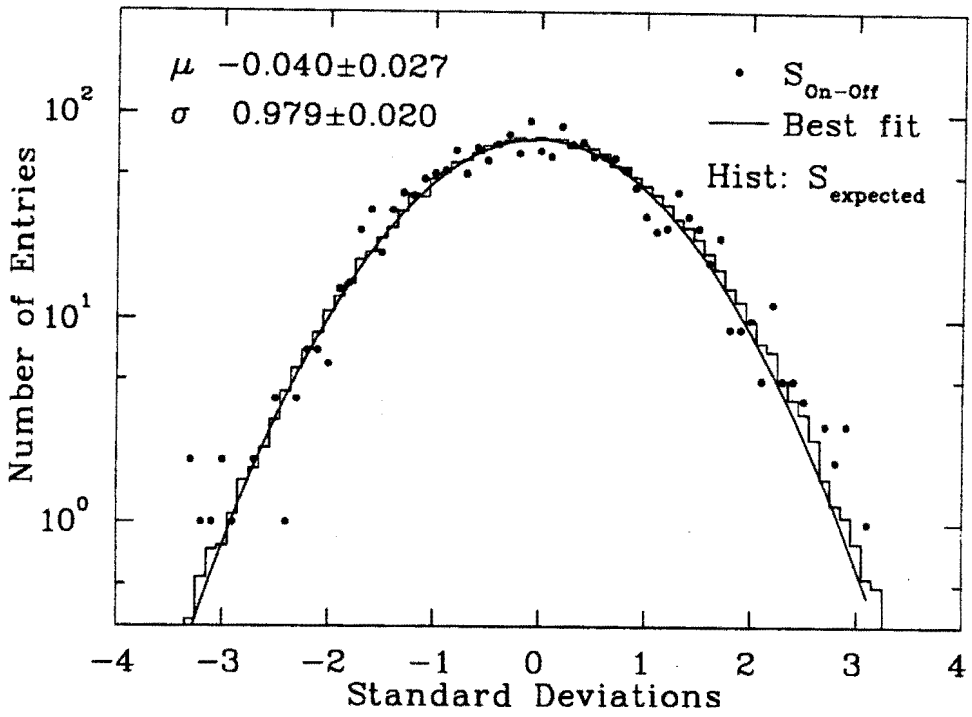

Figure 4.3: Distribution of the daily Li & Ma $S_{\text{on-off}}$ (points). μ and σ are the parameters of the best-fit gaussian (curve). The histogram is the distribution of $S_{expected}$ under H_0.

4.3 Search for Daily Emission

The N_{on} and N_{off} for every source-day are estimated by applying to the data the method described in the beginning of this chapter, and the significance $S_{\text{on-off}}$ gets calculated according to the Li & Ma prescription. 100 $S_{expected}$ get calculated, too, under the null hypothesis by applying 100 times to N_{off} the simulation described in section 4.2. The $S_{\text{on-off}}$ and the 100 $S_{expected}$ for each source-day in the data set are histogrammed. The best-fit gaussian to the $S_{\text{on-off}}$ distribution is also determined. Figure 4.3 shows all this information.

The fit of the distribution of $S_{expected}$ to that of $S_{\text{on-off}}$ has χ^2 of 79.3 with 61 degrees of freedom (probability 0.058) and the fit of the gaussian to $S_{\text{on-off}}$ has

χ^2 of 75.8 with 58 degrees of freedom (probability 0.058). No day exhibits $S_{\text{on-off}}$ deviating from what is expected under H_0. The *hottest day* has 47 events on-source where 27.8 are expected in a 2.0° bin, leading to $S_{\text{on-off}} = 3.1$ and post-trial probability (taking into account all the source-days searched) of 0.95 for falsely rejecting H_0. This implies a 90% confidence level upper-limit of 28.3 events from 4U 0115+63 for an episodic emission on the timescale of a day, and a corresponding upper-limit of $1.3 \times 10^{-12}\,\text{cm}^{-2}\text{s}^{-1}$ for the flux above 130 TeV (see section 3.4 for the calculation method).

4.4 Comparison of Different Implementations of Background Estimation

The backgound estimation method (see page 43) is based on a randomization. Therefore, different implementations of the same method or altogether different methods which still use a randomization procedure, should arrive at different background estimations. A slight variation in the implementation would be to initialize the random number generator to a different seed. A different method would be instead of picking for each event a new time from the observed set of event times, to pick a new (θ, ϕ) from the observed distribution of (θ, ϕ) (Alexandreas 1991b). Then each method would result in a different excess or deficit observed from a source for, as an example, each source-day. But if the background methods are free from errors, then the difference $S_1 - S_2$ of their daily significances should have a distribution that, under the assumptions of H_0, one should be able to calculate from purely statistical arguments. This would be a valid check of the methods.

It is obviously assumed that the two methods to be compared estimate the background for the same source in the sky; therefore their respective on-source bins

and their on-source sets of events should have at least some overlap or they should be identical. For simplicity we will treat the case where the on-source bin of one of the methods completely contains that of the other method. The ratio of the areas of the two bins is $\alpha(> 1)$; for identical bins $\alpha = 1$. Then, in the gaussian limit, $S_1 - S_2$ would be normally distributed with mean 0 and standard deviation

$$\sigma_{\Delta S} = 2 + \frac{2}{n} - \frac{2}{\sqrt{\alpha}},$$

where n is the number of fake (background) events created for each observed event.

The implementation used in the analysis presented here will be compared to a different implementation that is being used by the CYGNUS collaboration for a search for daily emission from about 50 point sources on the northern hemisphere sky. This second method uses a fixed-size square bin 2.0° in declination, and estimates the background by randomization every data run, i.e. four times a day. The method used here uses a variable-size bin that crudely averages between 2.05° and 2.1°, and calculates the background only once every source-day. Both methods use $n = 10$. Therefore we expect to get $\sigma_{\Delta S}$ between 0.499 and 0.543. Figure 4.4 shows the distribution of $S_1 - S_2$ for the daily excesses / deficits. The standard deviation of the best-fit gaussian agrees with the value expected for $S_1 - S_2$. The χ^2 of the fit is 40.1 with 34 degrees of freedom (probability 0.22).

The method used here has also been applied by using a fixed 2.0° bin. Then $S_1 - S_2$ has a distribution very similar to that of figure 4.4, and the best-fit gaussian has mean -0.023 ± 0.010, standard deviation 0.4404 ± 0.0073 and χ^2 32.3 with 32 degrees of freedom (probability 0.45). In this case of identical on-source bins, the value expected for $\sigma_{\Delta S}$ is 0.447.

The results of these comparisons show no problems with these background estimation methods.

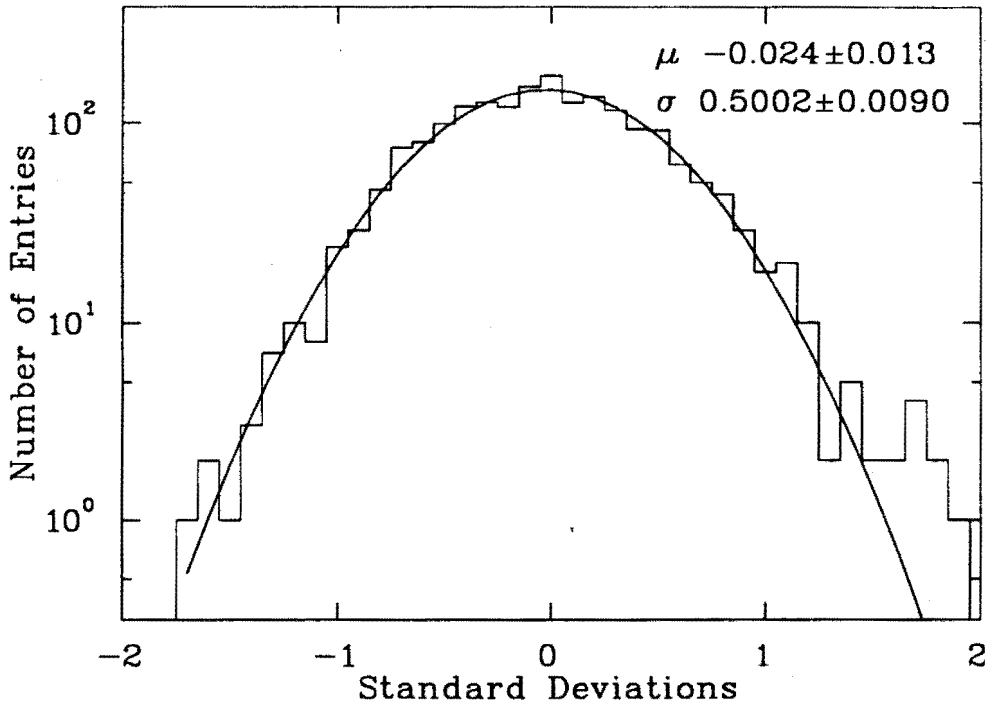

Figure 4.4: Distribution of the differences of the daily significances estimated by two different background methods (histogram). The legend gives the parameters for the best-fit gaussian (curve).

4.5 Search for Emission over Arbitrary Timescales

Table 4.2 shows the results of the search for emission over arbitrary timescales. The number of windows is the number of the independent (non-overlapping) time windows searched for a given timescale. This number and the factor for shifting each window sequence by 50% of the length of a window constitute the trials factor taken into account in the probabilities quoted here. The best probability for rejecting H_0 is for the 162 source-days long window and a 1.9° bin; taking into account that seven timescales have been searched, the final probability is $1-(1-0.20)^{1+6/2}=0.59$ for falsely rejecting H_0. This implies a 90% confidence level upper-limit of 112.5 events from 4U 0115+63 and a corresponding upper-limit of $1.6\times10^{-13}\,\mathrm{cm^{-2}s^{-1}}$ for the flux above 130 TeV. Table 4.2 gives $N_{90\%}$ and the flux upper-limit for the other

Time-scale (source -days)	Number of windows	N_{on}	N_B	S	Proba-bility	$N_{90\%}$	Flux < 10^{-12} (cm^2s sr)$^{-1}$
2	1034	88	60.3	3.2	0.76	40.1	0.81
6	363	124	88.9	3.3	0.24	49.9	0.69
18	125	216	173.5	3.0	0.29	62.1	0.44
54	43	1113	1041.2	2.1	0.72	116.9	0.14
162	13	918	846.3	2.3	0.20	112.5	0.16
486	4	2870	2793.7	1.4	0.41	151.1	0.066
1458	2	14481	14554.7	-0.6	0.94	167.6	0.014

Table 4.2: The most significant excess in each of the timescales searched. The number of the independent (non-overlapping) time windows is quoted. This number and the factor for shifting each window by 50% have already been taken into account in the probabilities quoted.

timescales, as well.

4.6 Search for Continuous Emission

Over the whole data-set available, 37267 events are observed in a 1.9° bin centered on 4U 0115+63 where 37520.7 are expected from the background, indicating a deficit equivalent to -1.3σ. The upper-limit calculation can still be used, and yields at most 213.6 events from 4U 0115+63 at the 90% confidence level, and a corresponding upper-limit of $7.0 \times 10^{-15}\,cm^{-2}s^{-1}$ for the flux above 130 TeV.

4.7 Search for Continuous Unpulsed Emission vs. Orbital Phase

The orbital phase of 4U 0115+63 (24.3 days) is so long that any emission occuring, due to the high eccentricity, at preferred points of the orbit, can only be observed

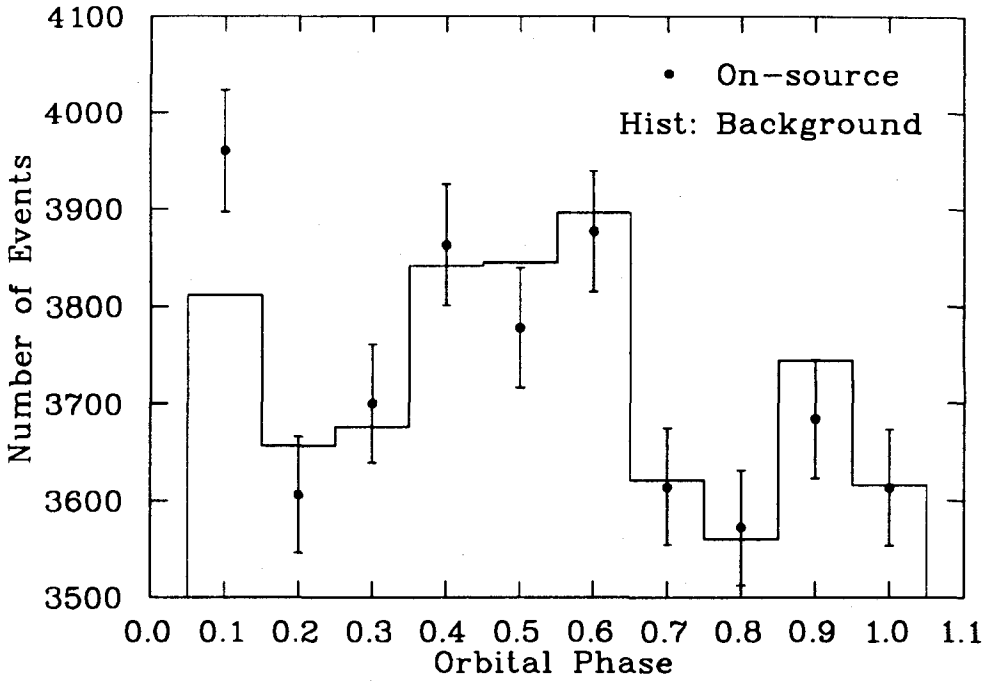

Figure 4.5: Distribution of the orbital phases of the on-source events (points), and of the background events (histogram). The statistical errors are indicated.

by a telescope with a high duty cycle. This is not the case with Čerenkov telescopes. The CYGNUS telescope, with its long operation, has a chance to detect such an emission if present.

The method of *epoch folding* is used here. The phases of all the on-source and background events, over the entire data set, that lie in the 1.9° bin centered on the source are determined according to the equation

$$\phi(t_{event}) = \phi(t_0) + \frac{t_{event} - t_0}{P_{orbital}}.$$

No ephemeris (epoch of orbital phase zero) has been established for 4U 0115+63. Thus t_0 is taken to be the time of the periastron passage (table 1.1). A different choice of t_0 would amount to a "rotation" of the phases around the circle that represents one orbital period. Figure 4.5 shows the distribution of the orbital phases

of the on-source events (points), and of the background events (histogram). The statistical errors are indicated. The background has been normalized to the number of counts in the on-source histogram. The bins are not uniformly populated because in the early days of operation attention was not paid to avoiding down-times when 4U 0115+63 was above the horizon. This resulted in non-uniform exposure over the orbital cycle. The fit of the on-source histogram to the background has χ^2 of 8.1 with 10 degrees of freedom (probability 0.62). The hottest bin has 3960 events on-source where 3811.4 are expected, leading to $S = 2.3$ (according to Li & Ma) and probability of 0.011. Since there are ten bins in the histogram, and also a 25-bin histogram has been examined (and did not show any larger excess in any bin), a trials factor of 20 is involved resulting in a probability of 0.20. This implies a 90% confidence level upper-limit of 233.5 events from 4U 0115+63 and a corresponding upper-limit of $7.5 \times 10^{-14}\,\mathrm{cm}^{-2}\mathrm{s}^{-1}$ for the flux above 130 TeV.

Chapter 5

Search for Pulsed Emission

The position of the (suspected) source in the sky is the only parameter known about the source that is employed in the search for unpulsed emission: if the source does emit at a level stronger than the background in the part of the energy spectrum being investigated here, then the flux detected from the on-source region should be stronger than that expected from the background. As presented in the previous chapter, this is not the case for 4U 0115+63 in the data that was examined. Other known source parameters can be used in trying to discriminate between the portion of the on-source set of events that is due to background and the rest, if any, which will be the signal from the source. As mentioned in section 1.3, in many detections in the X-ray region and some in the TeV - PeV region, the arrival times of the signal events from pulsars have a periodicity related to the spinning of the neutron star. If this period is known, it can be used as the signal characteristic to search for in the on-source data set. The arrival times of the on-source events are tested for phase allignment at the expected period, and the results are compared to what is expected under H_0. The latter is determined by testing the arrival times of the off-source events for phase allignment. Among the various test statistics available, the Rayleigh Power (RP) is found to be the most effective when the pulse profile shows

a single wide peak (de Jager 1987). This appears to be the case for 4U 0115+63 at least in the X-ray region (Whitlock 1989). This chapter presents the results of the application of the Rayleigh periodicity test to the data from the direction of 4U 0115+63.

5.1 Barycentering Corrections to Event Arrival Times

Before any phase allignment can be searched for, the Doppler effect contribution due to any relative motion between the source and the observer has to be subtracted from the event arrival times. The motions involved here are that of the earth in the solar system, and that of the 4U 0115+63 pulsar in the binary orbit with its companion. The arrival times observed at the telescope have to be reduced to the respective barycenters of these orbits (Slane 1988). The accuracy necessary in these calculations is dictated by the magnitude of the period one is searching for. The arrival times have to be established with accuracy comparable to a small fraction of the period of the pulsar in order to be able to determine whether the event phases are alligned or not.

The solar system barycentering correction consists of two terms: The first one is the propagation time of the signal from the telescope site to the solar system barycenter. It has to account for the position of the telescope on the earth, and the location of the earth with respect to the solar system barycenter. In order to gain full accuracy, the presence of all the heavy solar planets has to be taken into account and the orbit of the earth cannot be simplified to a binary one around the sun. This term has an approximately yearly sinusoidal variation with amplitude 500 s (about the size of the orbit of the earth). The second term is a general

relativistic correction to the clock time in order to account for the variations in the gravitational potential around the orbit of the earth; it has a yearly sinusoidal variation with amplitude about 1.66 ms and a semiannual one with amplitude 14 μs. Two solar system barycentering routines have been compared: one compiled by J. L. Evans and G. Dion (Dion 1992) for the CYGNUS collaboration, using routines from the library SLALIB (by P. T. Wallace, Rutherford Appleton Laboratory), and one compiled by R. March (1985) for the Haleakala collaboration. They both calculate both corrections mentioned above to the best known accuracy by using the positions and velocities of the earth relative to the solar system barycenter as calculated by the Jet Propulsion Laboratory and the U.S. Naval Observatory (JPL DE200 planetary ephemeris). The two routines have been found to agree to within 150 μs. R. March's routine has been found to agree, within 10 ms, to an independent one by MIT that is using the older MIT PEP311 planetary ephemeris instead of the DE200. G. Dion's routine has been found in agreement, within 1 ms, with the Jodrell Bank barycentering examples.

If the pulsar is in binary orbit with a companion star, then the event arrival times need to be corrected by the propagation time of the signal from the point of emission, assumed to be somewhere near the pulsar, to the barycenter of the binary orbit. The correction has a periodic variation with period equal to that of the binary orbit. If the orbit is a circle, as is almost the case with Hercules X-1, the variation is sinuoidal and the amplitude is equal to the radius of the orbit expressed in light-seconds. In the case of 4U 0115+63 where the orbit is eccentric, the correction follows the same principle but gets computationally a bit more involved because of the shape of the orbit and of the fact that the relation between the time and the angular position in the orbit has to be inverted via a numeric calculation in the absence of an analytic solution. The routine used here is the one used by the Whipple collaboration (Lamb 1990). For 4U 0115+63 the amplitude of the

correction is about 140 seconds (see table 1.1).

5.2 The Rayleigh Test

Among the many tests available for checking phase allignment of event arrival times, two are used in this dissertation: the *epoch folding* and the *Rayleigh test.*

The epoch folding method was outlined and used in section 4.7. It is used when the period P at which emission is expected is well known. This period may not be constant in time, but $P(t)$ has to be known. In this general case, the phase of an event that arrived at time t is given by:

$$\phi(t) = \phi(t_0) + \int_{t_0}^{t} \frac{dt'}{P(t')}.$$

In many cases P is satisfactorily approximated as being either constant or varying linearly with time with a known first time derivative $\dot{P}$. The problem of nonuniform exposure of section 4.7 is not present when searching for pulsar periods of the order of seconds or milliseconds. Then the distribution of the phases of the on-source events, often called the *light curve*, is expected under H_0 to be uniform within Poisson errors. The χ^2 test can be used to test for deviation from uniformity, or from the background phase distribution if available, or from light curves determined from previous measurements in the same or another energy range. The method of epoch folding can be applied, for example, to the Crab pulsar where the period is very well known. A problem with the method is that the results and their significance depend strongly on the t_0 used for phase zero, in the absence of an ephemeris established by previous observations, and on the number of bins used. Trials factors have to be "paid" for trying different numbers of bins.

When $P(t)$ is not known, one has to search for phase allignment by trying various P over an expected range, and to properly account for the trials involved.

The Discrete Fourier Transform can be used to check for the presence of a periodicity in the event arrival times: these can be considered as the nonuniform sampling of a function of time which is equal to the constant 1 (Slane 1988). The Rayleigh test statistic, the *Rayleigh Power* (RP) z, is equal to the magnitude of the complex Fourier amplitude of the sinusoidal component of frequency $\nu = P^{-1}$ in this function, divided by the number N of the arrival times t_i:

$$z(\nu) = \frac{1}{N}\left[\left(\sum_{i=1}^{N}\cos 2\pi\nu t_i\right)^2 + \left(\sum_{i=1}^{N}\sin 2\pi\nu t_i\right)^2\right].$$

Under H_0, i.e. if the t_i are random, $2z(\nu)$ follows, for large values of N, a χ^2 distribution with two degrees of freedom (the sine and the cosine sums; Mardia 1972), and the probability that a RP higher than a given value z is observed is given by (Greenwood 1955):

$$\Pr(>z|H_0) = e^{-z}\left[1 + \frac{2z - z^2}{4N} - \frac{24z - 132z^2 + 76z^3 - 9z^4}{288N^2} - \frac{1440z + 1440z^2 - 8280z^3 + 4890z^4 - 870z^5 + 45z^6}{17280N^3}\right].$$

This formula is accurate down to the probability level of 10^{-5} for $N \geq 14$ and to 10^{-3} for $N \geq 7$. For $N > 100$ one can omit the correction polynomial terms inside the square brackets.

If the time series t_i is of a finite duration T, frequencies ν less than $1/T$ apart are not statistically independent. This is equivalent to the optical diffraction patterns created by a single slit: The finite sequence t_i can be thought of as created from an infinite one on which one has superimposed a rectangular window function of length T. The frequency spectrum of this window function looks like a sinc function and gets superimposed on each of the frequencies in the sequence t_i. Even if the latter spectrum is discreet, it will become continuous after this superposition (convolution). The quantity $1/T$ is called the *Independent Fourier Spacing* (IFS). When searching over a frequency range, if the RP gets calculated only for frequencies

which are further apart than one IFS, the trials factor involved is the number of these independent frequencies. One would like, though, to *oversample* the spectrum, i.e. to calculate the RP even within one IFS in order to better locate a peak, if any. In this case, the trials factor can be expressed as the product of the number of independent frequencies and an effective correction factor due to oversampling. The latter depends on the periodicity test, the number of frequencies searched within one IFS, the number of the independent frequencies in the search range, and the value of the test statistic (the RP here). It is expected to saturate to a fixed value as the oversampling increases. In the case of the Rayleigh test, the oversampling trials factor saturates at about 3 (de Jager 1987).

5.3 Application of the Rayleigh Test to the Data

According to the most recent X-ray ephemeris (see section 1.3 and table 1.1), the pulsar period of 4U 0115+63 is 3.614690 s (ν = 0.2766489 Hz). During the X-ray emission outbursts that occur every about 3 years, the pulsar exhibits a spin up with observed $\dot{P}/P \approx -2 \times 10^{-4}\mathrm{yr}^{-1}$. But the period value measured during the various outbursts in the last twenty years is relatively the same (amounting to $10^{-6}\mathrm{yr}^{-1} < \dot{P}/P < 10^{-5}\mathrm{yr}^{-1}$), implying a spin down during the quiescent states between bursts. Observations of Hercules X-1 in the TeV and PeV energy range (Lamb 1988; Resvanis 1988; Dingus 1988b) showed a pulsar period significantly different (0.16%) from the X-ray period. The period search strategy motivated by these facts and followed here is that adopted by the Whipple Collaboration (Macomb 1991): For each timescale in which emission is searched for, two frequency ranges (two hypotheses) are examined:

Narrow range 0.2765659 Hz - 0.2767319 Hz, $\delta\nu/\nu = \pm 3 \times 10^{-4}$, motivated by the observed $\dot{P}$ during the X-ray bursts.

Wide range 0.2758190 Hz - 0.2774788 Hz, $\delta\nu/\nu = \pm 3 \times 10^{-3}$, motivated by the observed differences between X-ray and TeV periods in Hercules X-1.

The longer the time window in which emission is searched for, the shorter the IFS and the more frequencies for which the RP will be calculated in the narrow or wide range. For example, in the search for pulsed daily emission, where the longest exposure to the source is about 0.6 days, the minimum IFS is 20 μHz. In order to oversample at least 20 times, each frequency range is scanned in steps of 1 μHz; this means 166 (1660) frequencies in the narrow (wide) range. If one wanted to search windows 60 days long, the IFS would be 100 times smaller and, using the same oversampling, he would have to scan 100 times the number of frequencies used for daily emission search. The computation becomes very time-consuming. It has been decided that emission be searched over the timescales of a day, bacause that is the longest continuous exposure to the source, and of thirty days, motivated by the X-ray detections (Whitlock 1989; Tamura 1992). For 30-day long windows over the entire data set, only the narrow frequency range is scanned and in steps of 80 nHz, resulting in 5 times oversampling and 2075 frequencies.

For each of the time windows in a given timescale, and for each of the eleven times series (the on-source set and the ten background sets of events) the RP gets calculated at each of the frequencies tried. It gets calculated only if the corresponding series has at least 7 events. (For daily emission, this reduced the number of available days from 1960 to 1692). The probability to observe the resulting or higher RP is calculated and, if the calculation can be trusted for the given number of events, it is histogramed either in an on-source or in an off-source histogram as appropriate. After going through all the time windows in a given timescale, the histograms get converted into integral ones, and the first bin of the background histogram gets normalized to that of the on-source one. The on-source distribution

is then compared to the off-source one which is the expected under H_0.

Figure 5.1 shows the probability distributions for both search ranges in the timescale of one source-day, and for the narrow search range in the thirty-day long windows. In all cases, the on-source and background distributions agree very well. Their deviations from the uniform distribution at lower probabilities is the underestimation due to oversampling explained earlier.

5.4 Search for Continuous Pulsed Emission

If the emission duty factor of the source is low, then only one or a few time windows, of duration equal to the emission burst, would exhibit a RP anomalously high when compared to the background. According to figure 5.1, this is not the case. Previous claims of detection in the TeV energy region (Chadwick 1985; Brazier 1990) suggest, though, that the source is a continuous emitter, at least in that energy range and for the duration of those observations. If this is true in the 100 TeV region too, and since figure 5.1 does not show any deviation of the on-source distribution from the background one, the source must be emitting at a low level. A test sensitive to reveal such an emission is the *incoherent sum of the Rayleigh powers* from all the daily time windows (Lewis 1990). At each of the frequencies in the wide search range, the RPs from all the one-day long segments are added. Twice the incoherently summed power will follow, under H_0, a χ^2 distribution with twice the number of time windows as the degrees of freedom.

Figure 5.2 shows this incoherent sum for the on-source data, and for the background set that exhibits the maximum excursions from the value 1, expected under H_0. The highest average RP in the narrow (wide) range is 1.028 (1.085) with χ^2 probability of 0.12 (3.4×10^{-4}, but from the background sets it is apparent that even the highest average RP has a chance probability of about 10% due to the

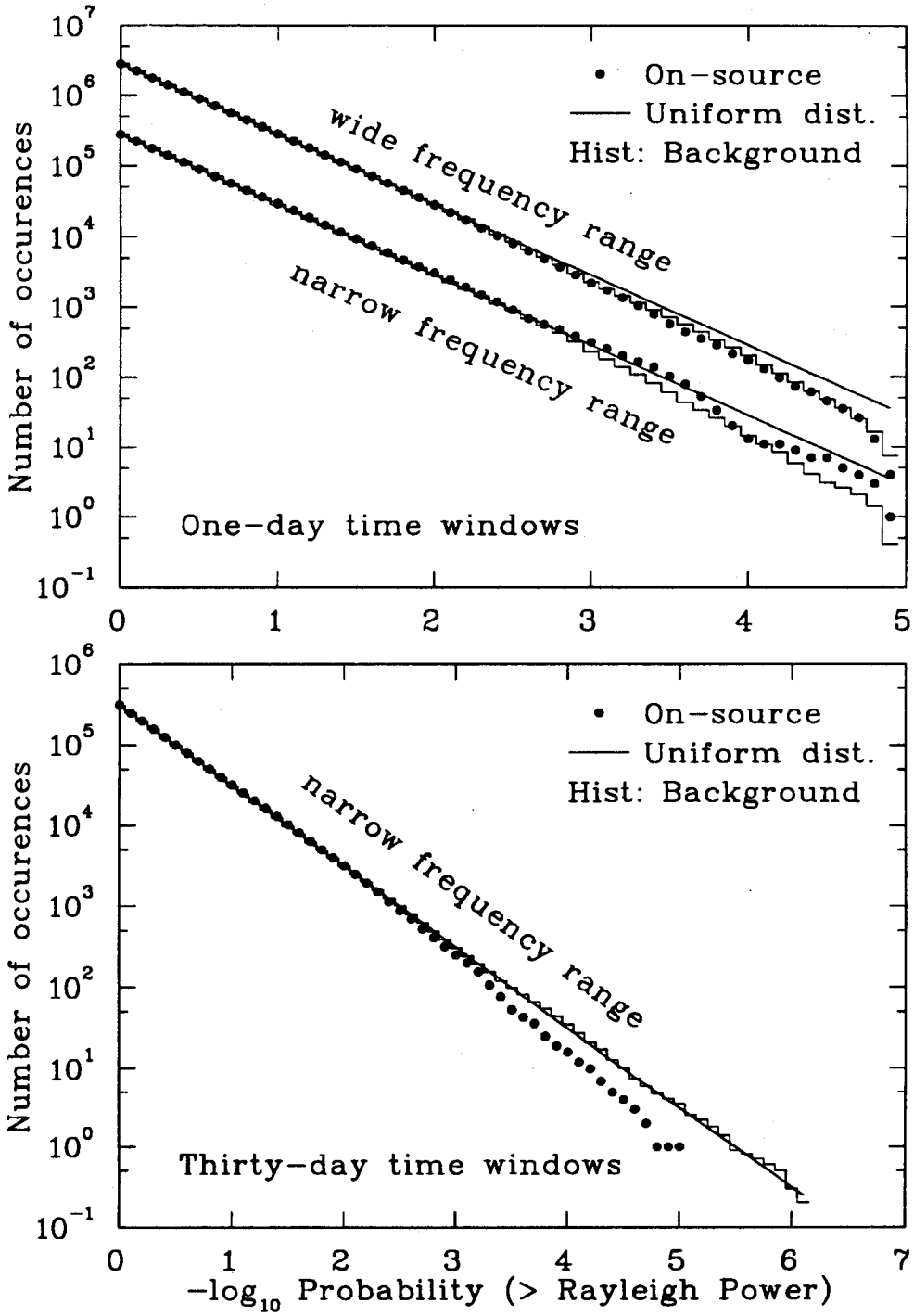

Figure 5.1: Distribution of the calculated probabilities of observing a given RP or higher, in the one-day and the thirty-day long time windows over the entire data set.

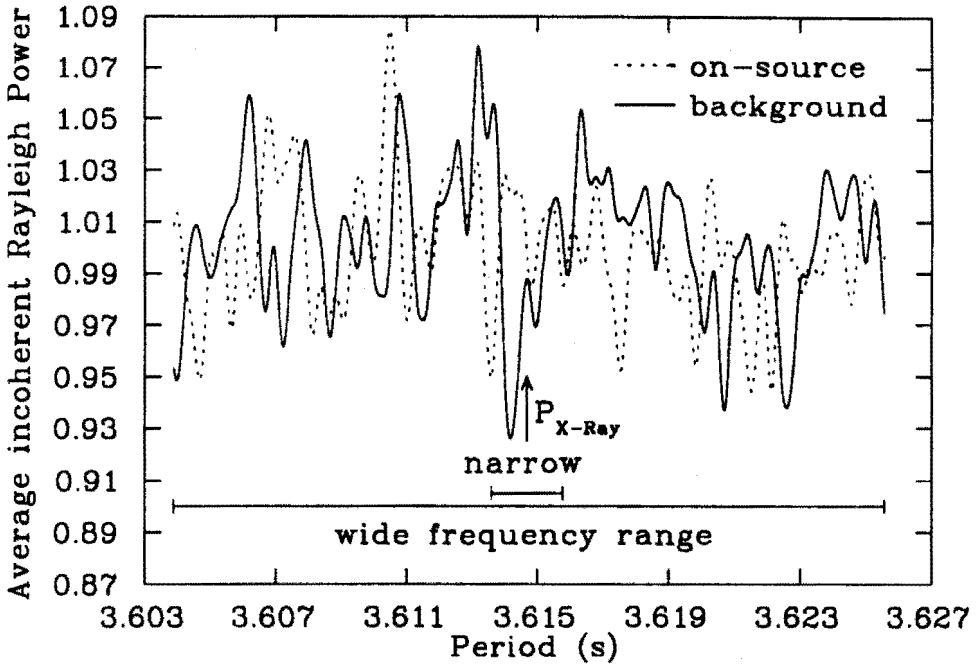

Figure 5.2: The spectrum of the incoherent sum, over all the one-day long time windows, of the RPs (divided by the number of windows), for the on-source and one of the background sets of events.

number of frequencies tried.

The incoherent sum of the RPs can be used to estimate an upper limit on the number of the events from the source (Lewis 1990). If N is the average number of on-source events in a day, and n_s is the average of the signal events, and g_s is the Fourier amplitude of the light curve (0.5 for a sinusoidal one), then if $N \gg n_s$, and the number of trials (days) is $M \gg 1$, the average incoherently summed RP P is normally distributed with expectation and standard deviation given by:

$$E = 1 + \mu, \qquad \sigma = \sqrt{\frac{1+2\mu}{M}}, \qquad \text{where} \qquad \mu = \frac{(n_s g_s)^2}{N}.$$

The integration of the upper tail of the gaussian results in:

$$\alpha = \int_{-\infty}^{\frac{P_{max}-E}{\sigma}} \frac{e^{-x^2/2}}{\sqrt{2\pi}} dx,$$

where α is the confidence level and P_{max} the highest average incoherent sum of the RPs. $\alpha = 0.90$ results in $(P_{max} - E)/\sigma) = 1.28$. Substitution of the expressions for P_{max} and E in terms of μ results in a quadratic equation in μ. The physically acceptable solution is the one consistent with $P_{max} > E$.

In the $M = 1692$ days there are 51310 events, leading to an average of $N = 30.3$ events per day. The highest incoherent RP sums attained in the narrow (wide) range imply a 90% upper limit of 2.7 (3.8) signal events from the source and a corresponding upper limit of 1.3 (1.9) $\times 10^{-13}\,\mathrm{cm}^{-2}\mathrm{s}^{-1}$ for the steady flux above 130 TeV.

Chapter 6

Conclusions

No indication of either unpulsed or pulsed emission of UHE gamma-rays from 4U 0115+63, over timescales varying from one source-day to the entire data set, has been found in the CYGNUS 1 database. The most stringent upper limits for the flux from the source are those for unpulsed emission. At the 90% confidence level these limits for the flux above 130 TeV are $1.3 \times 10^{-12}\,\mathrm{cm}^{-2}\mathrm{s}^{-1}$ for sporadic daily emission and $7.0 \times 10^{-15}\,\mathrm{cm}^{-2}\mathrm{s}^{-1}$ for continuous emission. These can be compared with the ones deduced by past observations (see table 1.2), by using an assumed photon integral spectral index 1.76 to reduce all the flux values to the same energy threshold. After this procedure, the flux upper-limit for continuous emission derived here agrees with the values by the Whipple and the Pachmarhi collaborations, both using atmospheric Čerenkov telescopes, but is two orders of magnitude lower than the upper-limits of the air-shower arrays EAS Top and Plateau Rosa.

The motivation for this observation has been the previously claimed detection by the Durham group (Chadwick 1985) in the TeV energies. No star models available so far, can convincingly predict PeV radiation from 4U 0115+63. Taking into account the distance of 2.5 Kpc, the implied upper-limit for the total source luminosity is 2×10^{33} ergs/s.

References

Acharya, B. S., et al. 1990, in Proc. 21st Internat. Cosmic Ray Conf. (Adelaide) 2, 319.

Aglietta, M., et al. 1990, in Proc. 21st Internat. Cosmic Ray Conf. (Adelaide) 2, 345.

Allen, R. C., et al. 1992, Nucl. Instr. Meth. A311, 368.

Alexandreas, D. E., et al. 1990, Phys. Rev. Lett. 64, 2973.

Alexandreas, D. E., et al. 1991a, Phys. Rev. D 43, 1735.

Alexandreas, D. E., et al. 1991b, Ap. J. 383, L53.

Alexandreas, D. E., et al. 1992, Nucl. Instr. Meth. A311, 350.

Amenomori, M., et al. 1990, Nucl. Instr. Meth. A288, 619.

Bhat, P. N., et al. 1987, see R. J. Protheroe in Proc. 20th Internat. Cosmic Ray Conf. (Moscow) 8, 36.

Biller, S. 1992, Ph. D. dissertation, University of California, Irvine (in preparation).

Bloomer, S. D., et al. 1988, J. Phys. G 14, 645.

Brazier, K. T. S., et al. 1990, in Proc. 21st Internat. Cosmic Ray Conf. (Adelaide) 2, 379.

Burnett, T. H., et al. 1990, Ap. J. 349, L25.

Chadwick, P. M., et al. 1985, Astron. Astrophys. 151, L1.

de Jager, O. C. 1987, Ph. D. dissertation, Potchefstroom University, South Africa.

Dingus, B. L., et al. 1988a, Phys. Rev. Lett. 61, 1906.

Dingus, B. L. 1988b, Ph. D. dissertation, University of Maryland, College Park, report 88-253, and Los Alamos National Laboratory report LA-11431-T; p. 38.

Dion, G. 1992, Ph. D. dissertation, University of California, Irvine.

Domokos, G. & Kovesi-Domokos, S. 1988, Phys. Rev. D 38, 2833.

Domokos, G., et al. 1989, Phys. Rev. Lett. 63, 844.

Domokos, G. & Kovesi-Domokos, S. 1990, Johns Hopkins Univ. preprint: JHU-TIPAC-9003.

Dowthwaite, J. C., et al. 1984, Nature 309, 691.

Drees, M. & Halzen, F. 1988, Phys. Rev. Lett. 61, 275.

Drees, M., et al. 1989, Phys. Rev. D 39, 1310.

Forman, W., et al. 1976, Ap. J. 206, L29.
Greenwood, J. A. & Durand, D. 1955, Ann. Math. Stat. 26, 233.
Greisen, K. 1960, Ann. Rev. Nucl. Science 10, 63.
Haines, T. J. 1986, Ph. D. dissertation, University of California, Irvine; p. 293.
Harding, A. K. 1990, in Proc. Arkansas Gamma-Ray and Neutrino Workshop, ed. G. B. Yodh, D. C. Wold, & W. R. Kropp, Nucl. Phys. B, 14A, 3.
Helene, O. 1983, Nucl. Instr. Meth. 212, 319.
Hess, V. F. 1912, Phys. Z. 13, 1084.
Hillas, A. M. 1984, Nature 312, 50.
Kiraly, P. & Meszaros, P. 1988, Ap. J. 333, 719.
Lamb, R. C. & Weeks, T. C. 1986, Astrophys. Lett. 25, 73.
Lamb, R. C., et al. 1988, Ap. J. 328, L13.
Lamb, R. C. 1990, private communication: binary orbit barycentering routine.
Lewis, D. A. 1990, in Proc. Arkansas Gamma-Ray and Neutrino Workshop, ed. G. B. Yodh, D. C. Wold, & W. R. Kropp, Nucl. Phys. B, 14A, 299.
Linsley, J. 1987, in Proc. 20th Internat. Cosmic Ray Conf. (Moscow) 2, 442.
Lloyd-Evans, J., et al. 1983, Nature 305, 784.
Li, T. P. & Ma, Y. Q. 1983, Ap. J. 272, 317.
Macomb, D. J., et al. 1991, Ap. J. 376, 738.
March, R. 1985. Solar system barycentering routine compiled in 1985; used by CYGNUS after private communication with C. Sinnis in 1991.
Mardia, K. V. 1972, Statistics of Directional Data; Academic Press, London.
Morello, C., et al. 1990, in Proc. 21st Internat. Cosmic Ray Conf. (Adelaide) 2, 349.
Neshpor, Y. I., et al. 1980, Izv. Krym. Astrofiz. Obs. 61, 61.
Rannot, R. C., et al. 1990, in Proc. 21st Internat. Cosmic Ray Conf. (Adelaide) 2, 315.
Rappaport, S., et al. 1978, Ap. J. 224, L1.
Raubenheimer, V. C., et al. 1989, Ap. J. 336, 394.
Resvanis, L. K., et al. 1988, Ap. J. 328, L9.
Samorski, M. & Stamm, W. 1983a, Ap. J. 268, L17.
Samorski, M. & Stamm, W. 1983b, in Proc. 18th Internat. Cosmic Ray Conf. (Bangalore) 11, 244.
Slane, P. O. 1988, Ph. D. dissertation, University of Wisconsin, Madison.
Stepanian, A. A., et al. 1972, Nature Phys. Sci. 239, 40.
Tamura, K., et al. 1992, Ap. J. 389, 676.
Vacanti, G., et al. 1991, Ap. J. 377, 467.
Vladimirsky, B. M., et al. 1984, Izv. Akad. Nauk. SSSR, Ser. Fiz. 48, 2078.
Weeks, T. C. 1988, Phys. Rep. 160, 1.
Whitlock, L., et al. 1989, Ap. J. 338, 381.

*U.S. Government Printing Office: 1992-774-036/67052